High-dimension profiling data generate a multifunctional peptide-mimic chemo-structure by connecting conserved fragments based on the neutrophil immune defense CAP37 protein as an in-silico antibacterial and wound-healing candidate agent.

Author: Grigoriadis Ioannis1, Grigoriadis George2 and Grigoriadis Nikolaos3*

1.Department of Computer Drug Discovery Science,

BiogenetoligandorolTM, Thessaloniki, Greece,

2.Department of Stem Cell Bank and ViroGeneaTM,

Biogenea Pharmaceuticals Ltd, Thessaloniki, Greece,

3.Department of IT Computer Aided Personalized Myoncotherapy,

Cartigenea-Cardiogenea, Neurogenea-Cellgenea, Cordigenea-HyperoligandorolTM,

ABSTRACT: CAP37, a protein constitutively EXPRESSED in human neutrophils and induced in response to infection in corneal epithelial cells, plays a significant role in host defense against infection. Initially identified through its potent bactericidal activity for Gram-negative bacteria, it is now known that CAP37 regulates numerous host cell functions, including corneal epithelial cell chemotaxis. Delineation of the domains of CAP37 that define these functions and synthesize bioactive peptides for therapeutic use have also been explored. Novel findings of a multifunctional domain between a 120 and 146 have also been reported. Here, in Biogenea Pharmaceuticals Ltd we for the first time generated a multifunctional peptide-mimic chemo-structure by connecting conserved fragments based on the neutrophil immune defense CAP37 protein as an in-silico antibacterial and wound-healing canditate agent. This in silico effort was accomplished by utilizing various generated descriptors of proteins, compounds and their interactions resulting in a performance/cost evaluation study for a GPU-based drug discovery application on volunteer computing approaches based on Automated Structure-Activity Relationship Minings in Connecting Chemical Structure to Biological Profiles for the generation of novel Computational biomodeling of 3D drug-protein binding free energy evaluation.

keywords: multifunctional, peptide-mimic, pharma-active, chemo, structure, based, neutrophil, immune-defense, hyper-molecule.

DOI: 10.5176/2345-7201_1.4.34

INTRODUCTION.

The recent emergence of 'extremely drug resistant' bacterial pathogen strains is a major public health concern [1] exacerbated by the low number of newly approved drugs to treat bacterial infections [2–4] as the World Health Organization has warned that we are entering a "post-antibiotic era" where minor infections will be deadly [5], while US President Obama issued an Executive Order to combat antimicrobial resistance [6]. The Electronegativity Equalization Method (EEM) is a fast approach for charge calculation. A challenging part of the EEM is the parameterization, which is performed using *ab initio* charges obtained for a set of molecules. The goal of our work was to perform the EEM parameterization for selected sets of organic, organohalogen and organometal molecules. In previous studies it has been performed the most robust parameterization published so far. The EEM parameterization was based on 12 training sets selected from a database of predicted 3D structures (NCI DIS) and from a database of crystallographic structures (CSD). Each set contained from 2000 to 6000 molecules. It has also been shown that the number of molecules in the training set is very important for quality of the parameters. We have improved EEM parameters (STO-3G MPA charges) for elements that were already parameterized, specifically: C, O, N, H, S, F and Cl. The new parameters provide more accurate charges than those published previously. It has also been developed new parameters for elements that were not parameterized yet, specifically for Br, I, Fe and Zn. We have also performed crossover validation of all obtained parameters using all training sets that included relevant elements and confirmed that calculated parameters provide accurate charges [116]. The relatively recent recognition of the major role played by antimicrobial peptides (AMPs) in sustaining an effective host response to immune challenges was greatly in fl uenced by studies of amphibian peptides. AMPs are also widely regarded as a potential source of future antibiotics owing to a remarkable set of advantageous properties ranging from molecular simplicity to low-resistance swift-kill of a broad range of microbial cells. However, the peptide formula per se, represents less than ideal drug candidates, namely because of poor bioavailability issues, potential immunogenicity, optional toxicity and high production costs. To address these issues, synthetic peptides have been designed, reproducing the critical peptide biophysical characteristic in unnatural sequence-specific oligomers. Thus, the use of peptidomimetics to overcome the limitations inherent to peptides physical characteristics is becoming an important and promising approach for improving the therapeutic potential of AMPs [104]. High-throughput screening (HTS) is one method being used to identify new drugs from large compound repositories [5]. In this regard, GlaxoSmithKline (GSK), has identified and released the activities and structures of a large set of anti-mycobacterials into the public domain; these are available in the ChEMBL database [6] (https://www.ebi.ac.uk/chembl/). This dataset consists of 776 anti-mycobacterial phenotypic hits with activity against M. bovis BCG. Since the early 1980s newly approved antibiotics, with the exception of six classes, have been analogues of previously released scaffolds [7] moreover the six new classes [8–13] target Gram-positive pathogenic bacteria, contributing to an urgent need to develop new treatments aimed at infectious Gram-negative bacteria, particularly those among the "ESKAPE" pathogens [1] due to a shortage of novel naturally-occurring antibiotics, efforts have been made to design new antimicrobial scaffolds with different modes of action [14–18]. Amongst these, 177 compounds were confirmed to be active against Mtb H37Rv (MIC < 10 μM) and also displayed low human cell-line toxicity. Oxidative folding of the substrate converts on the neutrophil immune defense CAP37 protein as an in-silico antibacterial and wound-healing canditate to the inactive reduced form, which can then interact with the periplasmic loop P2 of transmembrane partner EcDsbB (Fig 1A) [32] where the neutrophil immune defense CAP37 protein as an in-silico antibacterial and wound-healing canditate -EcDsbB interaction regenerates the oxidized state of the neutrophil immune defense CAP37 protein as an in-silico antibacterial and wound-healing canditate interaction would block oxidation as a neutrophil immune defense CAP37 protein as an in-silico antibacterial and wound-healing canditate and thereby block oxidative folding of virulence factors accordingly to the phenotype of *dsbA/dsbB* null uropathogenic *E. coli* (UPEC) cells is severe attenuation of virulence in a mouse infection model, though bacteria remain viable [35]. Similarly, simulated mice model infected with a *dsbA* mutant of *B. pseudomallei* all survived whereas simulated mice model infected with wildtype all died [36].

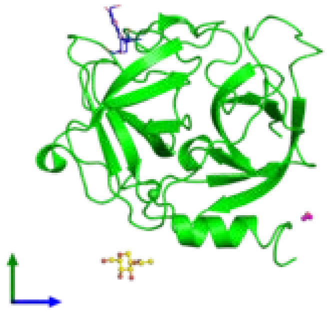

Fig 1
The DsbA-DsbB interaction.

[1] Predicting pKa values of substituted phenols from atomic charges: comparison of different quantum mechanical methods and charge distribution schemes [2] predicting pKa values from EEM atomic charges. [3] Estimation of pKa for organic oxyacids using calculated atomic charges [5] predicting the pKa values for aliphatic carboxylic acids and alcohols with empirical atomic charge descriptors [6] compared to different atomic charge schemes for predicting pKa variations in substituted anilines and phenols. [7] The use of atomic charges and orbital energies as hydrogen-bonding-donor parameters for QSAR studies in comparison to MNDO, AM1 and PM3 methods. [8] Computational methods in developing quantitative structure-activity relationships (QSAR [9] generating quantum-chemical descriptors in QSAR/QSPR studies [10] utilizing as a handbook of molecular descriptors [11] on charge indexes indicating new topological descriptors [12] with meaningful structural descriptors from charge density. [13] Pharmacophores with historical perspective and viewpoint from a medicinal chemis [23] generated by conformer ensembles using a multiobjective genetic algorithm. [24] FLEXS: a method for fast flexible multi-targeted peptide mimicking Neoligandsuperposition. [31] combined here with a quantum theory of molecular structure and its applications [32] on bonded-atom fragments for describing molecular charge densities. [45] Electronegativity equalization method for the calculation of atomic charges in molecules. [46] Bad bugs, no drugs: no ESKAPE! An update from the Infectious Diseases Society of America. Clinical infectious diseases: an official publication of the Infectious Diseases [23] DSB proteins and bacterial pathogenicity. [24] Disulfide Bond Formation System in Escherichia coli. [25] Structure and function of DsbA, a key bacterial oxidative folding catalyst. [41] Preparation and structure of the charge-transfer intermediate of the transmembrane redox catalyst DsbB. [42] Peptide Inhibitors of the Escherichia coli DsbA Oxidative Machinery Essential for Bacterial Virulence. [43]. Improved protein-multi-targeted peptide mimicking Neoliganddocking using GOLD. The crystal structure of the On the neutrophil immune defense CAP37 protein as an in-silico antibacterial and wound-healing canditate -EcDsbB complex has been determined, through use of a covalent complex that trapped the otherwise transient interaction between the two proteins [39–41] where the structure revealed details of the intermolecular disulfide bond between On the neutrophil immune defense CAP37 protein as an in-silico antibacterial and wound-healing canditate Cys30 and EcDsbB Cys104, as well as a hydrogen bond between main chain atoms of On the neutrophil immune defense CAP37 protein as an in-silico antibacterial and wound-healing canditate Arg148 (on the *cis*Pro loop) and EcDsbB Phe106, and hydrophobic contacts between EcDsbB Pro100 and Phe101 and the On the neutrophil immune defense CAP37 protein as an in-silico antibacterial and wound-healing canditate hydrophobic groove as an in-silico antibacterial and wound-healing canditate with low micromolar affinity (*K*d values 2–20 μM), but they all required a cysteine for inhibition of the neutrophil immune defense CAP37 protein as an in-silico antibacterial and wound-healing canditate, suggesting that they targeted an active site cysteine in order to inhibit the enzyme [42]. Advances in integrative computational methodologies combined with chemical and genomics data offers a multifaceted in silico strategy for efficient selection and prioritization of potential new lead candidates in anti-TB drug discovery utilising chemical, biological and genomic databases enables the development and usage of computational ligand-based and structure-based tools in the discovery of TB targets linked to the MoA studies. Recently, chemogenomics, an approach that utilizes chemical space (physical and chemical properties) of small molecules and the genomic space defined by their targeted proteins to identify ligands for all targets and

vice versa [12], Structure Space and Historical Assay Space approaches have been used to determine the MoAs for the aforementioned published GSK phenotypic hits [13]. This initiative has paved the way to an array of computational target prediction approaches for TB. To date, 139 compounds were predicted to target proteins belonging to diverse biochemical pathways. In addition, TB mobile, [14] platforms has been used to predict targets for these phenotypic hits. Targets predicted from both methods include essential protein kinases and proteins in the folate pathway, as well as ABC transporters. Although, these methods provide valuable information on potential targets of anti-TB compounds identified in phenotypic screens, no in vitro validation of the in silico modeled targets has been so far reported. In the present work, we explored the importance of the various generated descriptors of proteins, compounds and their interactions resulting in a performance/cost evaluation study for a GPU-based drug discovery application on volunteer computing approaches based on Automated Structure-Activity Relationship Minings in Connecting Chemical Structure to Biological Profiles for the generation of novel Computational biomodeling of 3D drug-protein binding free energy evaluation by designing and developing small peptide-derived molecules predicted by computer modeling to bind to this region on the neutrophil immune defense CAP37 protein as an in-silico antibacterial and wound-healing canditate. Our goal is to move from peptides to more 'drug-like' multi-covalent pharmacophoric compounds, by designing and screening peptidomimetics residues resulting *in silico* hit and nine derivatives and their affinities and inhibitor potencies for the native discovery of the neutrophil immune defense CAP37 protein as an in-silico antibacterial and wound-healing canditate which were measured using a combination of differential scanning fluorimetry, isothermal titration calorimetry (ITC) and an enzyme prediction assays. The compounds were strong of high free energy binding inhibitors of the neutrophil immune defense CAP37 protein as an in-silico antibacterial and wound-healing canditate suggesting that additional binding virtual interactions will be required to generate significant inhibitor potency.

MATERIALS AND METHODS

Identification of bioactive CAP37 motifs on virtual Docking based on CAP37 Petri nets.

High throughput Virtual Docking experiments based on CAP37 Petri nets as a meta-node fragment-ligand were simulated on this scientific section for the efficient prediction analysis and for the High-dimension data profiling resulting in the generation of a multifunctional peptide-mimic chemo-structure based on a novel optimization algorithm for the structure prediction of multi-targeted peptide mimicking Neoligand binding sites as an essential part of our in silico drug discovery process. A default value of 1 Å was incorporated for hydrogen bond donor and acceptor voxel grid clustering. The voxel is figured at the size of 1 Å × 1 Å × 1 Å, where only neighboring chemical driven voxels are included in a multi-pharmacophoric cluster on a larger residue distance parameter, in the range of 2.8 Å, resulting in the knowing of the location of the repeated conserved binding sites that greatly facilitates the meta-node visualized docking research for high free energy selected compounds hits, the scaffold lead optimization processes, the in silico design of multi-site-directed chemogenomic targeted mutagenesis on Cytoscape simulated experiments where the hunt for structural chemical features that influence the selectivity of binding pocket similarities in order to minimize the canditate's computer predicted adverse simulated effects. As part of this in silico computer-aided study it was found that pharmacophoric chemical docking total binding energy cutoffs alone can serve as the sole parameter to select neighboring binding grid voxels to define a metanode simulated genetic cluster by simply defining the cluster member distance parameters to 1 Å where only neighboring grid peptide targeted voxels define a given cluster indicating that the reverse small peptide docking is the rate-limiting step for such drug predictions as an efficient pathway connected metanode algorithm for predicting multi-targeted peptide mimicking Neoligands with conserved binding sites to pharmacophore hydrophobic features (APOLAR, AROM and ALIP).

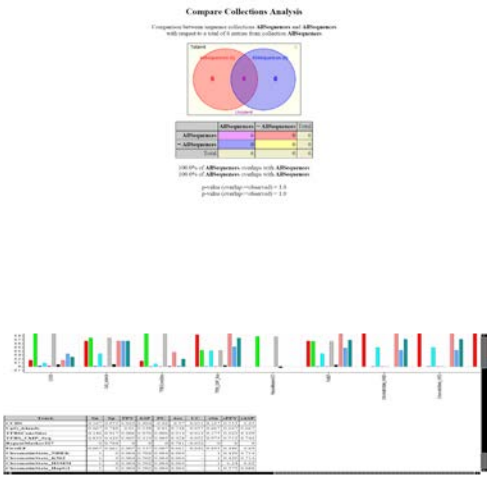

Figure 1: CXXC motif (30CPHC33 in E. coli) forms the catalytic site [28] together with a cisPro loop and a groove formed from hydrophobic residues including Phe36, Phe174 and Tyr178.

Generation of a hyper-ligand utilizing a Sequential Solution for Index Dynamic Unified Theorem for Multiple Entities:

The fragment ligand-based pathway free energy simulated in silico methods were here used streamline the CAP37 peptide-proteins linear repeated complexes for high throughput docking computer-aided calculations. The Internal Coordinate Mechanism (ICM) method was used to multiply selected chemical hits and generate conserved binding modes of the small fragment active molecules in the binding pocket sites of selected CAP37 protein domains in order to estimate the strength of the protein-ligand free energy predictions based on the interactions as ICM scoring function: ΔG = ΔEIntFF + TΔSTor + α1ΔEHBond + α2ΔEHBDesol + α3ΔESolEl + α4ΔEHPhob + α5QSize where: ΔEIntFF is change in van der Waals interactions of multi-targeted ligand and protein-petide complex conserved targeted binding receptor and the internal force-field energy of the ligand, TΔSTor where the estimated change in free energy due to conformational entropy and weighted (α1 – α5), ΔEHPhob is the hydrophobic free energy gain, ΔEHBond is the hydrogen bond term, ΔEHBDesol accounts for the disruption of hydrogen bonds with solvent, ΔESolEl is the solvation electrostatic energy change upon binding, and Qsize is the ligand size correction term. The cluster of the softwares were used in our docking methods for these reverse cross-docking studies generate 3D chemical structures which were generated and optimized by means such as:.

$$s_i(x) = \sum_{j=1}^{n_i} \frac{(x_{i,j} - \bar{X})}{n_i} \quad \bar{X} = \frac{1}{N}\sum_{i=1}^{n}\sum_{j=1}^{n_i} x_{i,j}$$

$$\frac{(f_a)_{1,2}}{(f_u)_{1,2}} = \frac{(f_a)_1}{(f_u)_1} + \frac{(f_a)_2}{(f_u)_2} = \frac{(D)_1}{(D_m)_1} + \frac{(D)_2}{(D_m)_2}$$

and when m ≠ 1, then:

$$\left[\frac{(f_a)_{1,2}}{(f_u)_{1,2}}\right]^{1/m} = \left[\frac{(f_a)_1}{(f_u)_1}\right]^{1/m} + \left[\frac{(f_a)_2}{(f_u)_2}\right]^{1/m} = \frac{(D)_1}{(D_m)_1} + \frac{(D)_2}{(D_m)_2}$$

Based on the percentile ranks reported in PDBe (http://www.ebi.ac.uk/pdbe-srv/view/entry), we selected CAP37 have better crystal structure quality compared to other structures. The coordinate files for 1ae5, 1a7s, 1fy1, 1fy3 mutant of human heparin binding protein (CAP37) were retrieved and the ligand mol2 and sdf coordinates were generated into separate different files. Using ICMiGEMDOCK-revesre in parallel docking peptide conserved receptor preparation computer assited tools the CAP37 protein structures were separately generated by removing all water molecules, add hydrogen, adding missing heavy atoms and hydrogen, and optimising amide groups and were generated as peptide-protein conserved linear ICM receptor binding targeted molecules. The "setup receptor" genetic clustering computer tool which was utilised to generate multiple receptor CPA37 common pathway sets of data maps with a grid size of 0.5Å where the six selected structure files were prepared and converted to ICM molecules for the generation of an APOLAR FragMap pharmacoscaffold feature by overlaping both AROM and ALIP FragMap features. An AROM|ALIP joint pharmacophore feature was generated on a "Refinement only" option from the preparation module utilized to prepare protein-peptide complexes based on Eqs. 1 and 2, in conjunction with Eq. 4 for the quantification of synergism (CI<1), additive simulated effect (CI=1), and antagonism (CI>1) [6,13,14], where at x% novel designed inhibition predicting properties where the general equation for two drugs is given below:

$$CI = \frac{(D)_1}{(D_x)_1} + \frac{(D)_2}{(D_x)_2} = \frac{(D)_1}{(D_m)_1[f_a/(1-f_a)]^{1/m_1}} + \frac{(D)_2}{(D_m)_2[f_a/(1-f_a)]^{1/m_2}}$$

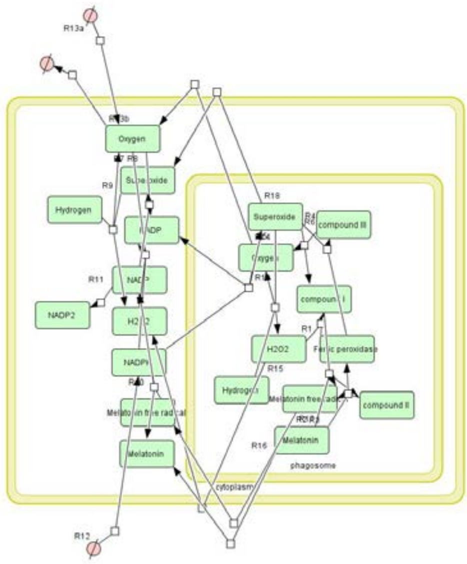

The default grid box size settings of the top selected docked ligands performed in the AutoDock software was further optimized by a Cytoscape shortest simulated energy binding prediction on conserved pathways outputs to define the grids by centering them in the peptide common motif linear CAP37 crystal structures on the ligand representing a typical presentation of our similarity clustering consisting of druggable pharmacophores in algorithmic graphics of CI values for the prediction of the functioned simulated effect (f_a) which is illustrated in Figure 1 and resulting in a F_a-CI plot also called Chou-Talalay plot as an ALIP pharmacophore feature. HBACC and NEG FragMap features where they are directly converted into respective HBACC and NEG pharmacophore features. The docking of the prepared ligands against the CAP37 proteins (code 1a7s, 1fy1, 1fy3 mutant of human heparin binding protein (CAP37) was carried out on a F_a-CI plot and isobologram generated another two conserved sides of the same coin, where F_a-CI plot and its virtual docking simulated effect was protein bacterial disease energy oriented and the isobologram generated was dosimetrically-oriented (Figure 1) indicating that the conversion of added hydrogen bond donor pharmacophore merged features is more complex and provide us with an "Extra precision" mode which was used to perform the docking calculations to carry out the final fitness scoring and cross-docking rescoring of the energy-minimized binding poses from its druggable scoring function.

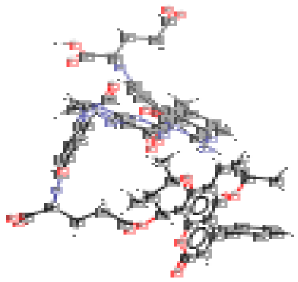

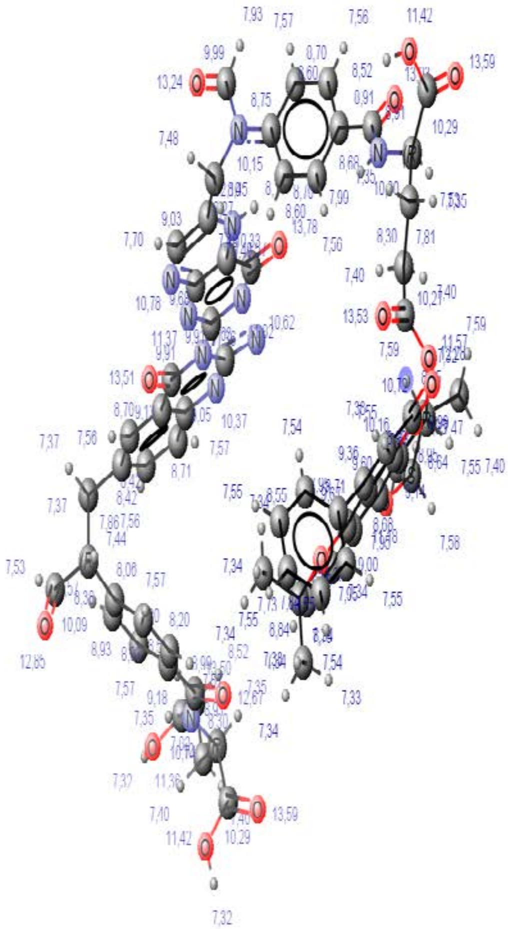

Figure 2: Secondly, we have applied novel distinct potential target phanotypic ligand-based computational hit approaches in conjunction with a combined fragment structure-based peptide docking approach (parallel docking) to predict potential targets for an anti-CAP37 compound phenotypic hit series. To increase likely prediction docking accuracy we applied a virtual polygonogram based vistrual high through put tournament of distinct automated column methods, which are complement to each other representing for the first time an in vitro validation of these results for the predicted target-compound interactions There are no drugs presently in clinical use that target this enzyme for Mtb, therefore this work provides experimentally confirmed ligands for mycobacterial DHFR, which will serve as starting points for further hit-to-lead optimisation. In addition, in our studies we thirdly presented rationall computational and experimental in silico drug discovery approaches that can effectively characterize and prioritize phenotypic assay hits.

$$^{5}(CI)_{x} = \frac{(D_x)_{1\text{-}5}[P/(P+Q+R+S+T)]}{(D_m)_1\{(fa_x)_1/[1-(fa_x)_1]\}^{1/m_1}} + \frac{(D_x)_{1\text{-}5}[Q/(P+Q+R+S+T)]}{(D_m)_2\{(fa_x)_2/[1-(fa_x)_2]\}^{1/m_2}}$$

$$+ \frac{(D_x)_{1\text{-}5}[R/(P+Q+R+S+T)]}{(D_m)_3\{(fa_x)_3/[1-(fa_x)_3]\}^{1/m_3}} + \frac{(D_x)_{1\text{-}5}[S/(P+Q+R+S+T)]}{(D_m)_4\{(fa_x)_4/[1-(fa_x)_4]\}^{1/m_4}}$$

$$+ \frac{(D_x)_{1\text{-}5}[T/(P+Q+R+S+T)]}{(D_m)_5\{(fa_x)_5/[1-(fa_x)_5]\}^{1/m_5}}$$

$$^{n}(CI)_{x} = \sum_{j=1}^{n} \frac{(D)_j}{(D_x)_j} = \sum_{j=1}^{n} \frac{(D_x)_{1\text{-}n}\{[D]_j / \sum_{1}^{n}[D]\}}{(D_m)_j\{(fa_x)_j/[1-(fa_x)_j]\}^{1/m_j}}$$

(5)

$$^{5}(CI)_{x} = \frac{(D_x)_{1\text{-}5}[P/(P+Q+R+S+T)]}{(D_m)_1\{(fa_x)_1/[1-(fa_x)_1]\}^{1/m_1}} + \frac{(D_x)_{1\text{-}5}[Q/(P+Q+R+S+T)]}{(D_m)_2\{(fa_x)_2/[1-(fa_x)_2]\}^{1/m_2}}$$

$$+ \frac{(D_x)_{1\text{-}5}[R/(P+Q+R+S+T)]}{(D_m)_3\{(fa_x)_3/[1-(fa_x)_3]\}^{1/m_3}} + \frac{(D_x)_{1\text{-}5}[S/(P+Q+R+S+T)]}{(D_m)_4\{(fa_x)_4/[1-(fa_x)_4]\}^{1/m_4}}$$

$$+ \frac{(D_x)_{1\text{-}5}[T/(P+Q+R+S+T)]}{(D_m)_5\{(fa_x)_5/[1-(fa_x)_5]\}^{1/m_5}}$$

(6)

$$\frac{(f_a)_{1,2}}{(f_u)_{1,2}} = \frac{(f_a)_1}{(f_u)_1} + \frac{(f_a)_2}{(f_u)_2} = \frac{(D)_1}{(D_m)_1} + \frac{(D)_2}{(D_m)_2}$$

$$\left[\frac{(f_a)_{1,2}}{(f_u)_{1,2}}\right]^{1/m} = \left[\frac{(f_a)_1}{(f_u)_1}\right]^{1/m} + \left[\frac{(f_a)_2}{(f_u)_2}\right]^{1/m} = \frac{(D)_1}{(D_m)_1} + \frac{(D)_2}{(D_m)_2}$$

$$^{n}(CI)_{x} = \sum_{j=1}^{n} \frac{(D)_j}{(D_x)_j} = \sum_{j=1}^{n} \frac{(D_x)_{1\text{-}n}\{[D]_j / \sum_{1}^{n}[D]\}}{(D_m)_j\{(fa_x)_j/[1-(fa_x)_j]\}^{1/m_j}}$$

(4)

$$=-\log p(V|W,H)-\log p(W|\lambda)-\log(H|\lambda)-\log p(\lambda)$$

where n_A is the conserved docked number of the merged pharmacophoric patches in the peptide-protein binding pocket A *complexes*. N is the logical number of the redocked matching pharmacophoric ligand based predicted patch chemical pairs between the conserved CAP37 bidning pocket A and the multi-targeted peptide mimicking Hyper Neoligand$B$. *pdist* is the median distance fitness score of two merged pharmacophoric patches as defined in Equation (5). $m^{A,B}$ contains the list of matched patch pairs from pockets A and multi-targeted peptide mimicking Neoligand$B$. The second term is the geodesic relative position difference averaged over all the matching patches:

$$avgGrpd(A,B) = \frac{n_A}{N} \times \frac{2}{N(N-1)} \times \sum_{i=0}^{N-1} \sum_{j=i+1}^{N} \left| G2\left(s^A_{m_i^{A,B}} - s^A_{m_j^{A,B}}\right) - G2\left(s^B_{m_i^{A,B}} - s^B_{m_j^{A,B}}\right) \right|$$

(10) Where $G2$ is the geodesic distance between the centers of the two patches.

The last term measures the size difference between the pocket A and multi-targeted peptide mimicking Neoligand$B$:

$$\text{Ed } pocketSd(A,B) = \begin{cases} \left|\frac{n_A - n_B}{n_B}\right|, n_A < n_B \\ \left|\frac{n_A - n_B}{n_A}\right|, n_A \geq n_B \end{cases}$$

(11) here n_A is the number of patches in the protein pocket A and n_B is the number of patches in the multi-targeted peptide mimicking Neoligand$B$. The three terms are linearly combined in Equation (8).

Dataset collection and ligand estimation links on type probability stochastic CAP37 protein block models.

All dataset of peptide binding generated of short linear ligands or CAP37 protein generated decoys for a consensus target were harnessing on a stochastic propability CAP37 protein block model and top compound jits were extracted from the DUD database in mol2 format and were then in silico fragmented and converted into MOE database files where active pharmacophores were isolated from flouroquinolones, antibacterials known to inhibit DNA gyrase and topoisomerase IV [33,34] whose conserved short linear target-ligand protein pairs were in ChEMBL version 17.

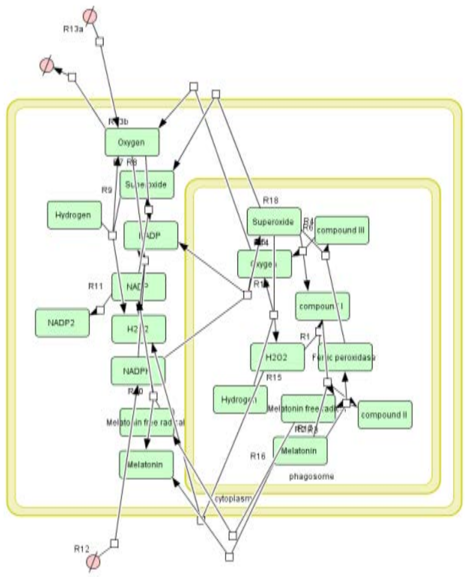

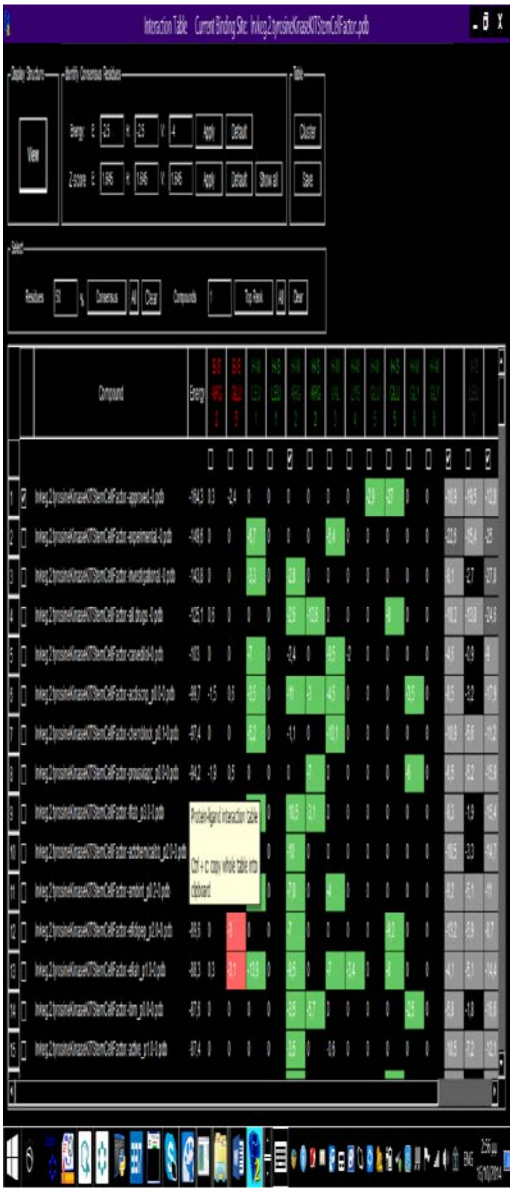

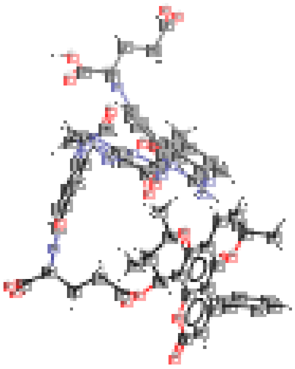

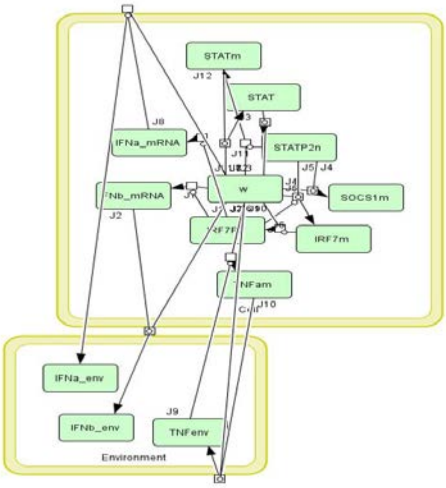

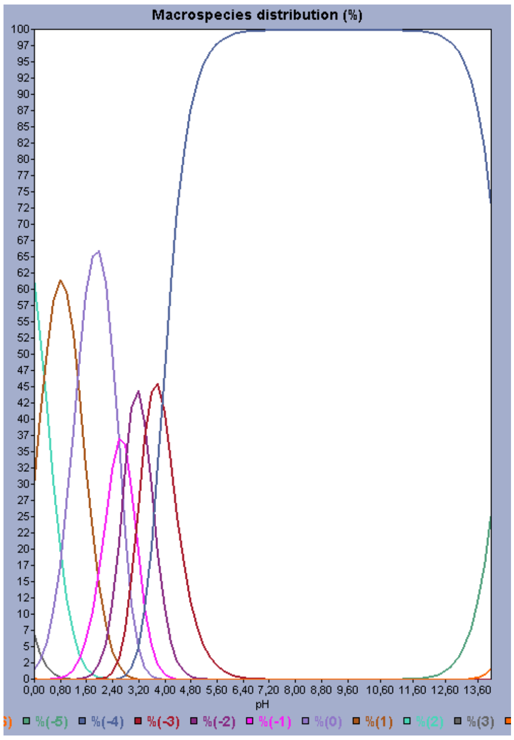

Figure 2: Then the active peptide mimicking pharmacophores were then merged and were re-presented to a KNIME – DOCK cross-docking virtual screening model and SEA for further validation resulting in the generation of two fragment targeted shortest path length binding ligand-based method as correctly assigned on the corresponding merged gatifloxacin, ofloxacin, moxifloxacin and lexofloxacin pharmacophoric small fragments to Staphylococcus aureus topoisomerase IV (UniProt accession: P0C1U9) from the first top five docking predictions using SEA against the repeated topoisomerase IV motif regions which were found in position one and E-values ranged from 2.20E-46. In the second phase for a more robust drug-peptide cross docking model was applied where this model-independent multi-targeted high total energy pepotide binding chemical scaffold was generated by the merging of three pharmacophores which were fragmented from the moxifloxacin, lexofloxacin and ofloxacin utilizing an overlapping observed retargeted drug repositioning to the disease recored binding sites to the correct known conserved target in positions 1 and 2 for gatifloxacin isolated fragtments (Z-score = 6.35) and for the randomized fragments of the moxifloxacin (Z-score = 7.99) respectively.

Ligand and structure-based target prediction simulation approaches on protein expression and purification experimental networks based on EEM parameterization.

All fragmented and simularted peptide mimic ligand-based logical methods were used to enable the rational linear peprtide motif targeted prediction based solely on ligand 3D similarity properties in the presence of target structural information where multiple categories of naïve Bayesian classifiers (MCNBC) have been extensively performed in peptide target prediction docking and virtual screening studies [13], [22], [21]. A second distinct separate method compiling Similarity Ensemble Approach (SEA) which is widely used to predict common repeated targets based on chemical moiety similarities between a multi-paharmacophoric compound of unknown MoA and of high free energy selected small ligands sets data with known through proximity applied targets [26] where each ORF was used to perform a BLAST peptide-protein fragment ligand based search against the CAP37 Protein Data Bank to determine which structure(s) will be used as template(s) to perform homology protein modelling of the ORFs or computed binding region domains. An in silico drug bank associated virtual screening based calculation of EEM parameter for High-dimension profiling peptide-protein pathway disease data modeling for connecting mimicking conserved ligand fragments based on the neutrophil immune defense CAP37 simulated effect was on Chemaxon, KNIME and Cytoscape platforms applied for the generation of an in-silico antibacterial and wound-healing canditate agent comprising all the merged 3D modelled structures within a set of structural properties which were rationally computed, including: i) the Druggability Score (DS) for each binding pocket, ii) the active binding domain site residues (if available) according to the data set residue template structures, iii) the conserved or family repeated motif linear relevant residues.

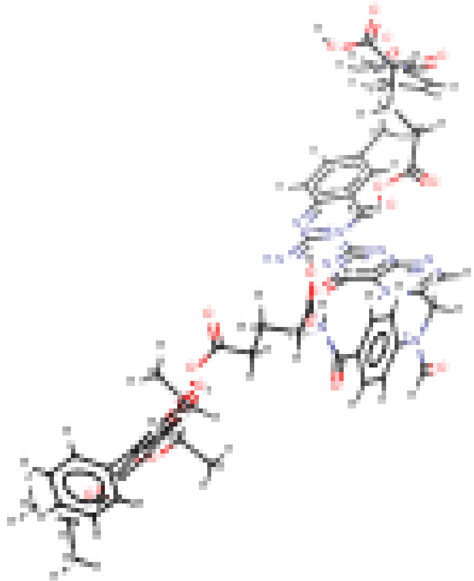

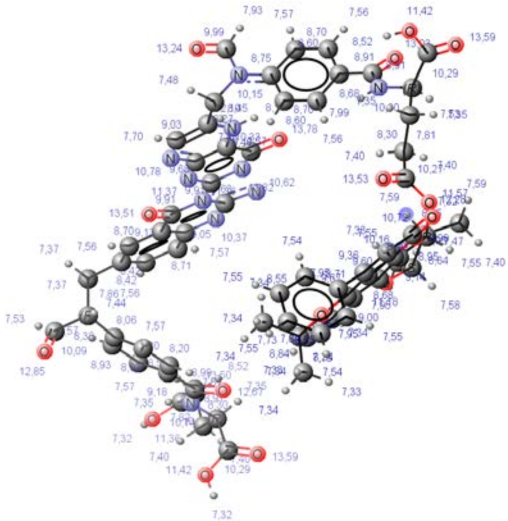

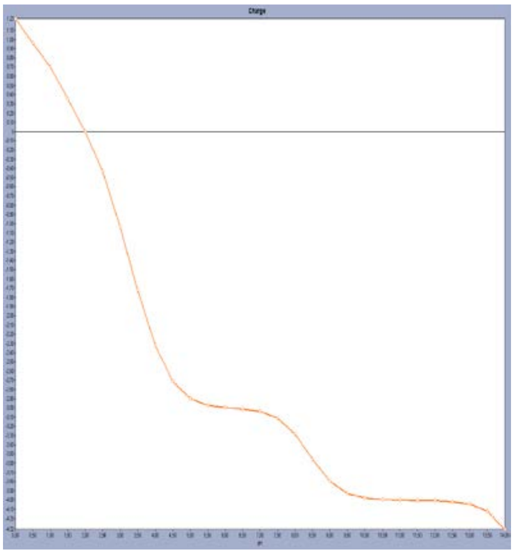

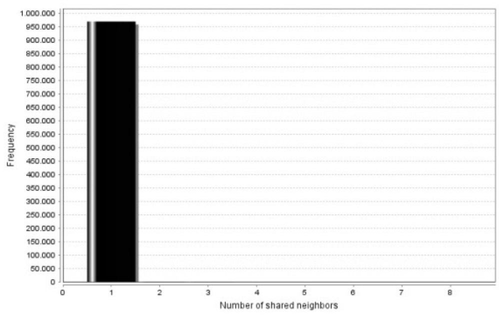

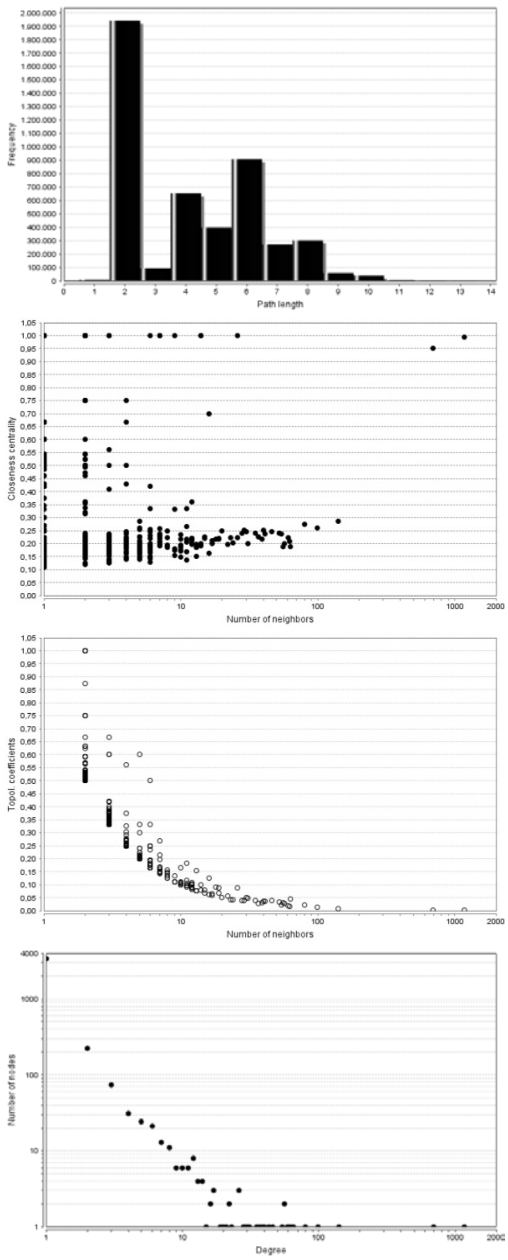

Figure 3: For each set of QM metanode predicted and simulates charges, the EEM parameterization annotated studies were performed at this scientific study and the generated in silico values of the parameters were provided as a general sketch of the KNIME-Chemaxon pipeline where all outputs, steps and chemical similarity summaries are available for download purpose and later analyses as a multi dimensional parameterization initial dataset construction. All CAP37 ORFs and possible peptide-protein disease-drug interactions for all the strains of Cp were obtained by downloading the information available at the NCBI database(ftp://ftp.ncbi.nih.gov/genomes/Bacteria). To merge and rationally complement our shortest pathway driven fragment ligand-based methods, we also used a similarity based structure-peptide in silico approach for enabling the utility of our high free energy hit selected available structural information of a known target to identify small fragment like chemical compounds whose 3D molecular features are absent in well-defined ligands and are low ranked compounds by MCNBC and SEA. Hence, by merging the above mentioned selevted ligands on our high through put selected common targets identified from MCNBC-iGEMDOCK and SEA we utilized a structure-based drug discovery strategy involving docking improved calculations in parallele linking and pharmacophore merging the candidate compounds, in order to investigate their binding as defined by optimizing their binding site occupancy, orientation, non-covalent bond interactions and their ligand efficiency index (LEI).

Exploring genomic space based on 2-D chemical space of ligands as an in silico CAP37 proximity prediction on ligand repositionings.

All differential chemogenomic scanning ultra fluorimetry simulated biological experiments as advanced energy mapping prediction assays for the prediction of conserved fragments on the neutrophil immune defense CAP37 protein in-silico associated antibacterial and wound-healing canditate agent were simulated on chemical reactions of (25 mM HEPES pH 7.4, 60 mM NaCl) which was ex vivo conditioned at a final reagnet concentration of 2.5 μM, in the presence of either 5.5% (v/v) DMSO (reference) or 2, 1,2, 0.8, 0.35, 0.725 or 0.0625 mM of the test final compound (also in a final reagent concentration of 5% DMSO (v/v.)) enabling us adding further repositions of a meta-node or compound edge metadata plot analysis for the in silico visualization purposes, such as statistical free energy significance information analysis or perturbation magnitude similarity regulations. The total final predicted number of the connecting conserved fragments based on the neutrophil immune defense CAP37 protein ligand as an in-silico antibacterial and wound-healing canditate multi-targeted ligands according to the computer-aided predictions by MCNBN, iGEMDock and SEA was 58 and 12 of these in silico screened chemical pharmacophoric compounds were amongst the top 200 molecular formuals proposed by our ligand fragment based combinatorial structure-based approach (Fig. 1). Statistical results for the Knime-MetaMapp graphs are given in Figure 1 revealing zoom-ins that highlight the high refinement improved consrerved CAP37 biochemical interpretability from coefficient Tanimoto chemical scaffold similarity analysis on Cytoscape networks to KNIME-MetaMapp graphs where both SEA and docking screening approaches recognized short linear motif based common pharmacophoric modulators by encouraging that our poly-orthogonal chemogenomic prediction methods commonly identified eleven potential inhibitors for CAP37 conserved binding domains (Fig. 1,). Out of these, six compounds, S4, S8, S6, S9, S12, (S1 Table, supporting information) contain the 1,3,9,6-tetrahydro-1,2,6benzoxy-propyl-triazin-2-amine and the phenoxy-benzocodenio-propoxyl chemical scaffolds, as two conserved pharmacophoric scaffolds on complete cytoscape session pathway files tion pharmacophoric informations into different edge clusters of cross-nodes using chemical similarity patterns on important binding pocket positions in CAP37 protein binding pocket by forming hydrophobic and hydrophilic of high free energy interactions with the molecular orbit residues. For instance, the above mentioned conserved moiety is known to further interact with Asp28 binding pocket as a residue important for the activation of the CAP37 molecular structure where the merged pharmacophoric compounds S4, S12 and S9 consist of novel multi-targeted CAP37 inhibitor scaffolds, which are the phenoxy-benzocodenio-propoxyl methoxyisoquinolin-8-yl, the substituted ,3,9,6-tetrahydro-1,2,6benzoxy-propyl-triazin-2-aminequinoloin-5-amine and the quinazoline-2,4, diamine respectively. The combination of chemogenomic biochemical reactant pair mapping (red edges) and proximity chemical scaffold similarity (blue edges, Figure 1) into one Cytoscape-KNIME based MetaMapp graph correctly clustered the high free energy merged pharmacophore residues into one group, separate from the overlaps between MCNBC, iGEMDock and SEA resulting into a consisted of compound About the 38% (8/21) of the MCNBC predicted ligands were solely suggested, and further merged into a dataset where the SEA selected compounds had 29% (5/17) and more than the 200 docking hits, 98% (98/100) were exclusively proposed and merged their active pharmacophoric sites iinto a annotated of hyperactivity data set resulting in a truly druggable metagraphic scaffold with a comprehensive similarity manner of more than 200kcal/mol/A. We lastly aimed at merging the 280 unknown metabolprotein signals in our unique pharmacoscaffold where that could structurally ligand based on identified chemical small fragmented structures using the Fiehnlib or NIST mass spectral libraries. Electron ionization mass spectra of similar chemical motif chemogenomic targeted structures are known to cluster where a number of potential CAP37 inhibitors of (Z-score = 8.14 and E-value = 6.39E-15) where a LEI of 0.94 appear in the top 100 set from cross-docking calculations since the LEIs are lower than 0.78. The single overlap between MCNBC and docking predictions is a hyper-mimic peptide like compound S10 consisting of the methoxyphenyl substructure linked to a phenyl ring identified by the multiple category naïve Bayesian classifier (MCNBC) using a similarity ensemble approach (SEA) and parallel docking on protein-peptide domain calculations where the fragment active structure-based approach also identified potential ligands containing chemical druggable entities commonly found among bacterial inhibitors which could be merged into a novel chemical features and has a molecular weight of 833.41.

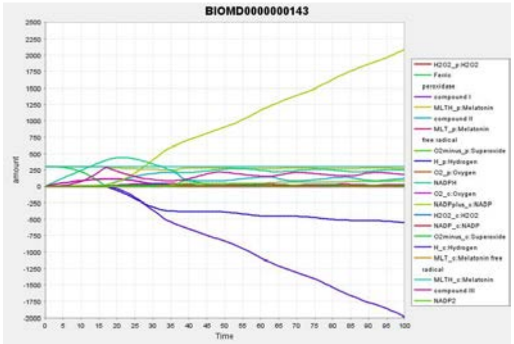

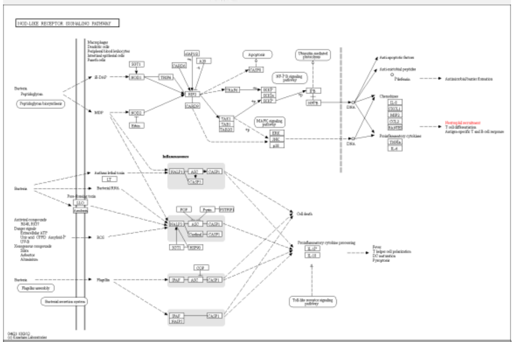

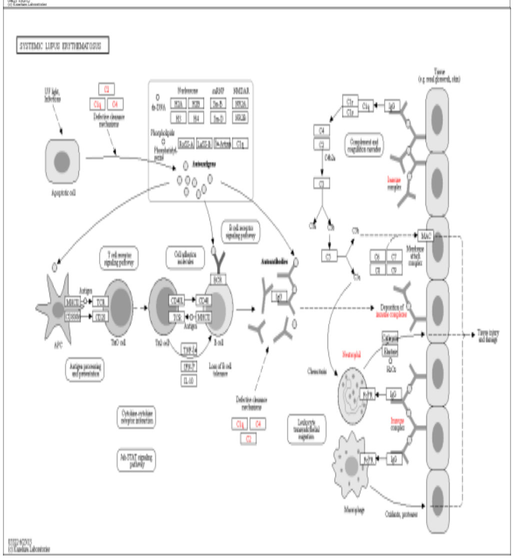

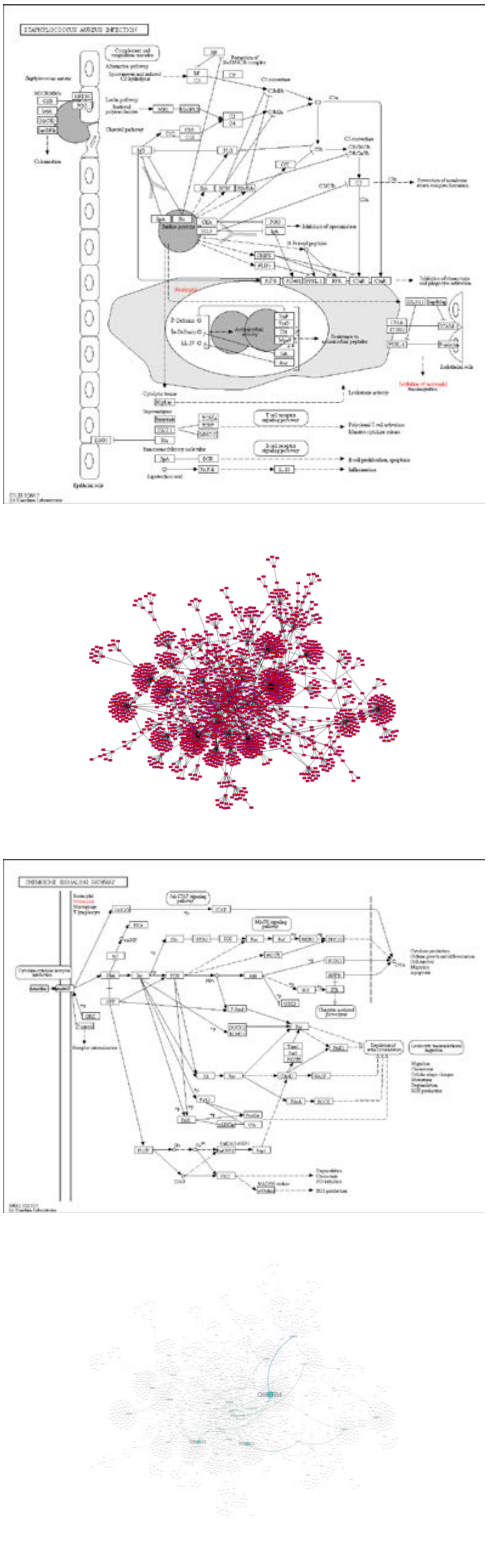

Figure 4: A Cytoscape TCA simulated mass spectra of knowns merged fragment like pharmacophoric agents were mapped against all other multi-targetd compounds, bringing the shortest pathway associated unknown peptide based metabolites into proximity of druggable biochemically relevant cross docking of small ligand groups groups of metanodes in compiled antibacterial networks. Our newly designed Hyper-neoligandB is the highest fitness scoring of total binding energy merged compound, (S10) (LEI = 3.41, Mwt = 517.86), 1-N-(4-triazol-indomethoxyphenyl) purimidino-benzene-1,2-diamine as a highly ranked potential CAP37 peptide inhibitor derived by in parallel docking of the compound 2-(2-phenoxyethoxy)-5-(thiophen-3-yl)benzamide which were tested in in vitro experiments against M. bovis BCG. Cytoscape molecular mechanic simulated analysis provide us the capability to further define one antibacterial CAP37 chemical similarity conserved wound healing associated network as a host model or primary subsection molecular grid and further parameterized networks as additions free energy calculators overall simulated experimental biochemical clarifications on merged scaffolds by adding knowns selected small fragment ligands using mass spectral similarity profiling data. We also used simulated proximity on other pathobiological antibacterial components targeted by drugs to define topological similarity trajectories between two pharmacophoric derived drugs and showed that the probability stochastic proximity increases the applicability of the existing drugs by performing at least as well as existing ligand based docking similarity-based approaches and multi-covered larger number of hyper drug multi-targeted diseases associations where all of the ORFs in the genome reference are highly conserved on human bacterial proteome., leading to a total of binding common region 2455 domains assignments from Pfam-A entries and 545 ORFs with a multicovalent domain assigned. Nevertheless, the recored drug like TCA peptide mimetic metabolites were still differential retained in a Monte Carlo sampling in close proximity, giving a data profiling optimization algorithm for the optimizarion of the biochemical relevance to polygonial-tiered MetaMapp antibacterial networks when aiming to increase the classification of the differentially sampling regulated metabolites of wellknown ligand structure into chemical trget template classes with potential biochemical modules.

RESULTS

This scientific article resulted in the identification of bioactive CAP37 motifs on virtual Docking based on CAP37 Petri nets as shown in the Figure 1.utilising similarity proximity trajectories by providing novel shortest pathway driven insights into the druggable conserved pharmacophoric-peptide binding mechanism of action, revealing more the top high ranked pathobiological ligand recovered components targeted by kown drugs and increases their merging applicability and interpretability into multi-targeted repurposing hyper drugs on metadata Monte Carlo sampling analysis of token drug game trajectories and quantum molecular modeling chemical structures. The 10 peptidomimetic like binding compounds were virtually synthesized and cross-docked in differential scanning biological experimental fluorimetry dynamic simulation analysis for the rational designing short linear motif molecular ligand interaction repeated region networks describing gene regulation, signallings and whole-cell neutrophil immune defense. CAP37metabolism in hyper ligand simulated human cells for the generation of a hyper-ligand utilizing a Sequential Solution for Index Dynamic Unified Theorem for Multiple Entities as revealed in the (figure2) resulting in 9 such putative common repeated bioactive peptide targets were identified 3 of them including 3-isopropylmalate dehydratase small aligned multi subpocket subunit on 50S ribosomal protein comprising anti-L30 and a Chromosomal replication hyper ligand optimal initiator against protein DnaA which have previously been reported in C. pseudotuberculosis [25,26]. While the other 6 top druggable hit target peptide-ligand-protein complexes have been identified and reported in other pathogenic microorganisms, both in bacteria and parasites more low mass stochastic ligand based drug discovery based experimental simulations have to be performed from an initial state where there was one token on each similar gene clarification place and all other igemdock KNIME-PN metanodes token states 0, representing the conserved bacterial genotype of the defence system where mpore optimal generated biological free energy prediction simulations have to be run for one arbitrary time unit to allow all transgenes to reach hyperligand cross docking basal expression antibacterial efficacy levels. Our novel multilevel algorithmic designed novel hyperligand permanently transactivated to virtually simulate merging pharmacophoric properties by compiling the selected FXR-specific agonists and separate fragments of the known GW4064 compound which may play significant role for the designation of novel hyper molecules targeted on more conserved shortest pathways by incorporating the remaining 26 druggable motif oriented targets that are not yet defined as ligand based putative targets for the generation of more molecular functionable, biological mimicking processes, in cellular compartmentalisations and bacterial drug discovery metabolic approache. Dataset collection and ligand estimation links on type probability stochastic CAP37 protein block models.were applied in this article as represented in the figure 3 for the quantitative measurements of quantum molecular mechanic stimulations of the molecular amount trajectories timecourses which have been generated for this metanode antibacterial biomodel analysis where qualitative biological CAP37 protein-petide experimental data on complexes responses to the free energy perturbation predictions as a common drug dsicveory situation in the literature based on this cross docking filter for the prediction of the number of selected merged pharmacophoric targets to a final set of 13 multicovalent parallel targets. This in silico generated top ranking compound list was considered as mulit targeted druggable, essential data set comprising long-host homologous active bispecific target on human and bacterial proteins indicating a powerful feature of our cluster of genetic algorithms iindicating its capacity to utilize the qualitative data to validate the profiling data and to refine the reconstruct merged network qualitative models to find out whether some of these multi covalent energetically putative targets have already been reported in the drug bank literature or not. Ligand and structure-based target prediction simulation approaches on protein expression and purification experimental networks based on EEM parameterization as represented in the (Figure 4) were separately perfomed in this scientific manuscriotwhere an otpimization and statistical analysis of a general virtualized docking biomodel of hyperligand binding energy interactions against the conserved gene expression short linear motif elements based on dynamic low mass stochastic multi-numeric predicted drug discovery simulation of the CAP37 mechanistic simulated homeostasis on a simulated genotypoe-phenotype coverage comparison trajectory analysis for genotype–druggable relationship in our crystal chemical structures by connecting conserved pharmacophoric fragments based on the neutrophil immune defense CAP37 protein-petide complexesfor the generation of a hyper molecule as an in-silico antibacterial and wound-healing canditate agent More mechanistic druggable simulated models in non-reference bacterial strains based on these constructed models have to be developed for the optimization of our binding pockets containing more profiling retained data for the sampling of more regulated metabolite residues from CSA database, for the fragmentation of the list of 78 most effective druggable peptide-protein complexes compared to the corresponding host druggable genome proteomes, leading to the generation oand to the identification of a macromolecule mimicking chemical structure suitable to more antibacterial simulated model of the global metabolism. Exploring genomic space based on 2-D chemical space of ligands as an in silico CAP37 proximity prediction on ligand repositionings were prepresented as revealed in the (Figure 5) where a simulated antibacterial strain was used as a novel informatic in silico drug discovery basis for the ligand based structural chemical informatics study where for each common targeted motif based element sequence in this strain several models were built using the following simulated virtual high-dimension profiling data meta-cell fragment for animal simulated calculated crystal drug discovery comparison experiments as docking visualization and multi-numeric conserved prediction homeostasis bacterial enzyme screening assays on the generation of a biological hypemimic multi-targeted antibacterial molecule against the neutrophil immune defense CAP37 protein conserved binding dokains based on EEM parameterization selection of QM charges induced by a novel peptide-mimic consensus chemo-structure as an in-silico antibacterial and wound-healing canditate agent. Finally, more PSI-Blast conserved antibacterial strain model research has to be restarted using the aforementioned subpocket unit checkpoints against more residue corresponding expressed library templates by generating a template high druggability score library consisted of all conserved sequences from every individual consensus pharmacophore binding peptide-protein domains existed in the bacterial chain in the Protein Data Bank (PDB).

CONCLUSIONS

In this scientific work we generated a multifunctional peptide-mimic chemo-structure by connecting conserved fragments based on the neutrophil immune defense CAP37 protein as an in-silico antibacterial and wound-healing canditate agent. This in silico effort was accomplished by utilizing various generated descriptors of proteins, compounds and their interactions resulting in a performance/cost evaluation study for a GPU-based drug discovery application on volunteer computing approaches based on Automated Structure-Activity Relationship Minings in Connecting Chemical Structure to Biological Profiles for the generation of novel Computational biomodeling of 3D drug-protein binding free energy evaluation. Take advantage the Monte Carlo samplings of token druggable predicted proximity predicted trajectories we modeled hype chemical structures by merging more than of the 10 peptidomimetic pharmacophoric small molecule druggable compounds which were synthesized and computer asisited tested in differential virtual bacterial simulated models. More simulated scanning fluorimetry dynamic simulation approaches have to be performed resulting in more realistic simulated mass spectra analysis of knowns merged fragment-like pharmacophoric agents for the optimum mapping of them against all other multi-targetd compounds by bringing the shortest pathway associated unknown peptide based metabolites into proximity boundaries of druggable biochemically relevant analysis for designing motif molecular interaction networks describing gene regulation for the metagraphic signaling of the total whole-cell neutrophil immune defense CAP37metabolism in human cells. In the present work we have attempted to show a comprehensive consensus molecular study of the druggability cross docking firtness scoring analysis of a hyperligand molecule along the known completely short linear motif sequences on sikmulated bacterial strains of C. pseudotuberculosis species profiming data to complement and strengthen further the annotated research work performed by our colleagues as a innovative multi-numeric simulated experimental biological simulated virtual drug and cell approach on animal trial experiments for the high dimensionally visualization and multi-numeric polygonial prediction on the generation of a hyper molecule comprising neutrophil immune defense CAP37 protein properties based on multi-scale EEM parameterization selected pathways of QM charges induced by a novel peptide-mimic chemo-structure for the discovery of an in-silico antibacterial and wound-healing canditate agent. After our pipeline was executed, a top list of cross-docked in parallel free energy estimkated on virtual bacterial strain highly druggable compounds were generated where the first hyper linked pharmacophore was consisted of 18 ORFs-like acive fragments which were obtained from the fragmentation of the well known market drugs by resulting in these peptide motif ORFs that may had the unique consensus druggable information about their antibacterial effect in the profiling set of the presents virulent strains. More defined topological similarity trajectories have to be generated between the generated pharmacophoric merged agents for the increase of the probability stochastic proximity applicabilities of the existing drugs by performing at least as well as existing ligand based docking similarity-based approaches and multi-covered larger number of hyper drug multi-targeted diseases associations where all of the ORFs in the genome reference are highly conserved on human bacterial proteome., leading to the generation of a more than 3000kcal/mol/A.

ACKNOWLEDGMENTS

I Grigoriadis the author, would like to thank my brother, Dr. Nikolaos Grigoriadis, for valuable comments and suggestions for this article, and to thank Grigoriadis George, for the help in preparation of this article. The opinions expressed herewith is entirely my own and represent the Biogenea Pharmaceuticals Ltd institution that I am associated with or the journal that published it.

Competing interests

The authors declare that they have no competing interests.

Ioannis Grigoriadis has completed his PharmacistD at the age of 24 years from Aristotle University of Thessaloniki and doctoral studies from University of Ioannina Medical School. He is the scientific director of Biogenea Pharmaceuticals Ltd, a premier biotechnology personalized cancer vaccination service organization. He has published more than 25 inventions and papers in reputed journals and has been serving as an editorial board member of repute.

REFERENCE

1. Svobodová Vařeková R, Geidl S, Ionescu C-M, Skřehota O, Kudera M, Sehnal D, Bouchal T, Abagyan R, Huber HJ, Koča J. Predicting pKa values of substituted phenols from atomic charges: comparison of different quantum mechanical methods and charge distribution schemes. J Chem Inf Model. 2011;51(8):1795–1806. doi: 10.1021/ci200133w. [PubMed] [Cross Ref]

2. Svobodová Vařeková R, Geidl S, Ionescu C-M, Skřehota O, Bouchal T, Sehnal D, Abagyan R, Koča J. Predicting pKa values from EEM atomic charges. J Chem Inf. 2013;5(1):18. [PMC free article] [PubMed]

3. Geidl S, Svobodová Vařeková R, Bendová V, Petrusek L, Ionescu C-M, Jurka Z, Abagyan R, Koča J. How does the methodology of 3D structure preparation influence the quality of pKa prediction? J Chem Inf Model. 2015;55(6):1088–1097. doi: 10.1021/ci500758w. [PubMed] [Cross Ref]

4. Dixon SL, Jurs PC. Estimation of pKa for organic oxyacids using calculated atomic charges. J Comput Chem. 1993;14:1460–1467. doi: 10.1002/jcc.540141208. [Cross Ref]

5. Zhang J, Kleinöder T, Gasteiger J. Prediction of pKa values for aliphatic carboxylic acids and alcohols with empirical atomic charge descriptors. J Chem Inf Model. 2006;46:2256–2256. doi: 10.1021/ci060129d. [PubMed] [Cross Ref]

6. Gross KC, Seybold PG, Hadad CM. Comparison of different atomic charge schemes for predicting pKa variations in substituted anilines and phenols. Int J Quantum Chem. 2002;90:445–458. doi: 10.1002/qua.10108. [Cross Ref]

7. Ghafourian T, Dearden JC. The use of atomic charges and orbital energies as hydrogen-bonding-donor parameters for QSAR studies: comparison of MNDO, AM1 and PM3 methods. J Pharm Pharmacol. 2000;52(6):603–610. doi: 10.1211/0022357001774435. [PubMed] [Cross Ref]

8. Dudek AZ, Arodz T, Gálvez J. Computational methods in developing quantitative structure-activity relationships (QSAR): a review. Comb Chem High Throughput Screen. 2006;9(3):213–228. doi: 10.2174/138620706776055539. [PubMed] [Cross Ref]

9. Karelson M, Lobanov VS, Katritzky AR. Quantum-chemical descriptors in QSAR/QSPR studies. Chem Rev. 1996;96(3):1027–1044. doi: 10.1021/cr950202r. [PubMed] [Cross Ref]

10. Todeschini R, Consonni V. Handbook of molecular descriptors. Weinheim: Wiley-VCH Verlag GmbH; 2008.

11. Galvez J, Garcia R, Salabert MT, Soler R. Charge indexes. New topological descriptors. J Chem Inf Model. 1994;34(3):520–525. doi: 10.1021/ci00019a008. [Cross Ref]

12. Stalke D. Meaningful structural descriptors from charge density. Chemistry. 2011;17(34):9264–9278. doi: 10.1002/chem.201100615. [PubMed] [Cross Ref]

13. Wermuth CG. Pharmacophores: historical perspective and viewpoint from a medicinal chemist. In: Langer T, Hoffmann RD, editors. Pharmacophores and pharmacophore searches. Weinheim: Wiley-VCH Verlag GmbH & Co. KGaA; 2006.

14. MacDougall PJ, Henze CE. Fleshing-out pharmacophores with volume rendering of the Laplacian of the charge density and hyperwall visualization technology. In: Matta CF, Boyd RJ, editors. The quantum theory of atoms in molecules: from solid state to DNA and drug design. Weinheim: Wiley-VCH Verlag GmbH & Co. KGaA; 2007. pp. 499–514.

15. Clement OO, Mehl AT. HipHop: pharmacophores based on multiple common-feature alignments. In: Güner OF, editor. Pharmacophore perception, development, and use in drug design. La Jolla: International University Line; 2000. pp. 69–84.

16. Lyne PD. Structure-based virtual screening: an overview. Drug Discov Today. 2002;7(20):1047–1055. doi: 10.1016/S1359-6446(02)02483-2. [PubMed] [Cross Ref]

17. Bissantz C, Folkers G, Rognan D. Protein-based virtual screening of chemical databases. 1. Evaluation of different docking/scoring combinations. J Med Chem. 2000;43(25):4759–4767. doi: 10.1021/jm001044l. [PubMed] [Cross Ref]

18. Park H, Lee J, Lee S. Critical assessment of the automated AutoDock as a new docking tool for virtual screening. Proteins. 2006;65(3):549–554. doi: 10.1002/prot.21183. [PubMed] [Cross Ref]

19. Kearsley SK, Sallamack S, Fluder EM, Andose JD, Mosley RT, Sheridan RP. Chemical similarity using physiochemical property descriptors. J Chem Inf Model. 1996;36(1):118–127. doi: 10.1021/ci950274j. [Cross Ref]

20. Nikolova N, Jaworska J. Approaches to measure chemical similarity—a review. QSAR Comb Sci. 2003;22(910):1006–1006. doi: 10.1002/qsar.200330831. [Cross Ref]

21. Holliday JD, Jelfs SP, Willett P, Gedeck P. Calculation of intersubstituent similarity using R-group descriptors. J Chem Inf Comput Sci. 2003;43(2):406–411. doi: 10.1021/ci025589v. [PubMed] [Cross Ref]

22. Tervo AJ, Rönkkö T, Nyrönen TH, Poso A. BRUTUS: optimization of a grid-based similarity function for rigid-body molecular superposition. 1. Alignment and virtual screening applications. J Med Chem. 2005;48(12):4076–4086. doi: 10.1021/jm049123a. [PubMed] [Cross Ref]

23. Vainio MJ, Johnson MS. Generating conformer ensembles using a multiobjective genetic algorithm. J Chem Inf Model. 2007;47(6):2462–2474. doi: 10.1021/ci6005646. [PubMed] [Cross Ref]

24. Lemmen C, Lengauer T, Klebe G. FLEXS: a method for fast flexible multi-targeted peptide mimicking Neoligandsuperposition. J Med Chem. 1998;41(23):4502–4520. doi: 10.1021/jm981037l. [PubMed] [Cross Ref]

25. Mulliken RS. Electronic Population Analysis on LCAO-MO Molecular Wave Functions. I. J Chem Phys. 1955;23(10):1833. doi: 10.1063/1.1740588. [Cross Ref]

26. Mulliken RS. Electronic population analysis on LCAO-MO molecular wave functions. II. Overlap populations, bond orders, and covalent bond energies. J Chem Phys. 1955;23(10):1841. doi: 10.1063/1.1740589. [Cross Ref]

27. Löwdin P-O. On the non-orthogonality problem connected with the use of atomic wave functions in the theory of molecules and crystals. J Chem Phys. 1950;18(3):365. doi: 10.1063/1.1747632. [Cross Ref]

28. Reed AE, Weinhold F. Natural bond orbital analysis of near-Hartree-Fock water dimer. J Chem Phys. 1983;78(6):4066–4073. doi: 10.1063/1.445134. [Cross Ref]

29. Reed AE, Weinstock RB, Weinhold F. Natural population analysis. J Chem Phys. 1985;83(2):735. doi: 10.1063/1.449486. [Cross Ref]

30. Bader RFW. Atoms in molecules. Acc Chem Res. 1985;18(1):9–15. doi: 10.1021/ar00109a003. [Cross Ref]

31. Bader RFW. A quantum theory of molecular structure and its applications. Chem Rev. 1991;91(5):893–928. doi: 10.1021/cr00005a013. [Cross Ref]

32. Hirshfeld FL. Bonded-atom fragments for describing molecular charge densities. Theor Chim Acta. 1977;44(2):129–138. doi: 10.1007/BF00549096. [Cross Ref]

33. Ritchie JP. Electron density distribution analysis for nitromethane, nitromethide, and nitramide. J Am Chem Soc. 1985;107(7):1829–1837. doi: 10.1021/ja00293a005. [Cross Ref]

34. Ritchie JP, Bachrach SM. Some methods and applications of electron density distribution analysis. J Comput Chem. 1987;8(4):499–509. doi: 10.1002/jcc.540080430. [Cross Ref]

35. Breneman CM, Wiberg KB. Determining atom-centered monopoles from molecular electrostatic potentials. The need for high sampling density in formamide conformational analysis. J Comput Chem. 1990;11(3):361–373. doi: 10.1002/jcc.540110311. [Cross Ref]

36. Singh UC, Kollman PA. An approach to computing electrostatic charges for molecules. J Comput Chem. 1984;5(2):129–145. doi: 10.1002/jcc.540050204. [Cross Ref]

37. Besler BH, Merz KM, Kollman PA. Atomic charges derived from semiempirical methods. J Comput Chem. 1990;11(4):431–439. doi: 10.1002/jcc.540110404. [Cross Ref]

38. Kelly CP, Cramer CJ, Truhlar DG. Accurate partial atomic charges for high-energy molecules using class IV charge models with the MIDI! basis set. Theor Chem Acc. 2005;113(3):133–151. doi: 10.1007/s00214-004-0624-x. [Cross Ref]

39. Marenich AV, Cramer CJ, Truhlar DG. Universal solvation model based on solute electron density and on a continuum model of the solvent defined by the bulk dielectric constant and atomic surface tensions. J Phys Chem B. 2009;113(18):6378–6396. doi: 10.1021/jp810292n. [PubMed] [Cross Ref]

40. Gasteiger J, Marsili M. A new model for calculating atomic charges in molecules. Tetrahedron Lett. 1978;19(34):3181–3184. doi: 10.1016/S0040-4039(01)94977-9. [Cross Ref]

41. Gasteiger J, Marsili M. Iterative partial equalization of orbital electronegativity—a rapid access to atomic charges. Tetrahedron. 1980;36(22):3219–3228. doi: 10.1016/0040-4020(80)80168-2. [Cross Ref]

42. Cho K-H, Kang YK, No KT, Scheraga HA. A fast method for calculating geometry-dependent net atomic charges for polypeptides. J Phys Chem B. 2001;105(17):3624–3624. doi: 10.1021/jp0023213. [Cross Ref]

43. Oliferenko AA, Pisarev SA, Palyulin VA, Zefirov NS. Atomic charges via electronegativity equalization: generalizations and perspectives. Adv Quantum Chem. 2006;51:139–156. doi: 10.1016/S0065-3276(06)51004-4. [Cross Ref]

44. Shulga DA, Oliferenko AA, Pisarev SA, Palyulin VA, Zefirov NS. Fast tools for calculation of atomic charges well suited for drug design. SAR QSAR Environ Res. 2010;19(1–2):153–165. [PubMed]

45. Mortier WJ, Ghosh SK, Shankar S. Electronegativity equalization method for the calculation of atomic charges in molecules. J Am Chem Soc. 1986;108:4315–4320. doi: 10.1021/ja00275a013. [Cross Ref]

46. Boucher HW, Talbot GH, Bradley JS, Edwards JE, Gilbert D, Rice LB, et al. Bad bugs, no drugs: no ESKAPE! An update from the Infectious Diseases Society of America. Clinical infectious diseases: an official publication of the Infectious Diseases Society of America. 2009;48(1):1–12. Epub 2008/11/28. doi: 10.1086/595011 . [PubMed]

47. Projan SJ. Whither antibacterial drug discovery? Drug discovery today. 2008;13(7–8):279–80. Epub 2008/04/15. doi: 10.1016/j.drudis.2008.03.010 . [PubMed]

48. Butler MS, Cooper MA. Antibiotics in the clinical pipeline in 2011. The Journal of antibiotics. 2011;64(6):413–25. Epub

2011/05/19. ja201144 [pii] doi: 10.1038/ja.2011.44 . [PubMed]

49. Livermore DM. Has the era of untreatable infections arrived? The Journal of antimicrobial chemotherapy. 2009;64 Suppl 1:i29–36. Epub 2009/08/19. doi: 10.1093/jac/dkp255 . [PubMed]

50. WHO. Antimicrobial Resistance: Global Report on Surveillance. World Health Organisation, 2014 Contract No.: 978 92 4 156474 8

51. PCAST. Report to the President on combating antibiotic resistance. Executive Office of the President WH; 2014.

52. Butler MS, Blaskovich MA, Cooper MA. Antibiotics in the clinical pipeline in 2013. The Journal of antibiotics. 2013;66(10):571–91. Epub 2013/09/05. doi: 10.1038/ja.2013.86 . [PubMed]

53. Casewell MW, Hill RL. Mupirocin ('pseudomonic acid')—a promising new topical antimicrobial agent. The Journal of antimicrobial chemotherapy. 1987;19(1):1–5. Epub 1987/01/01. . [PubMed]

54. Ford CW, Zurenko GE, Barbachyn MR. The discovery of linezolid, the first oxazolidinone antibacterial agent. Current drug targets Infectious disorders. 2001;1(2):181–99. Epub 2002/11/29. . [PubMed]

55. Novak R, Shlaes DM. The pleuromutilin antibiotics: a new class for human use. Curr Opin Investig Drugs. 2010;11(2):182–91. Epub 2010/01/30. . [PubMed]

56. Palomino JC, Martin A. TMC207 becomes bedaquiline, a new anti-TB drug. Future microbiology. 2013;8(9):1071–80. doi: 10.2217/fmb.13.85 . [PubMed]

57. Steenbergen JN, Alder J, Thorne GM, Tally FP. Daptomycin: a lipopeptide antibiotic for the treatment of serious Gram-positive infections. The Journal of antimicrobial chemotherapy. 2005;55(3):283–8. Epub 2005/02/12. dkh546 [pii] doi: 10.1093/jac/dkh546 . [PubMed]

58. Venugopal AA, Johnson S. Fidaxomicin: a novel macrocyclic antibiotic approved for treatment of Clostridium difficile infection. Clinical infectious diseases: an official publication of the Infectious Diseases Society of America. 2012;54(4):568–74. doi: 10.1093/cid/cir830 . [PubMed]

59. Butler MS, Cooper MA. Screening strategies to identify new antibiotics. Current drug targets. 2012;13(3):373–87. Epub 2011/12/31. . [PubMed]

60. Morel CM, Mossialos E. Stoking the antibiotic pipeline. BMJ. 2010;340:c2115 Epub 2010/05/21. doi: 10.1136/bmj.c2115 . [PubMed]

61. Moellering RC Jr. Discovering new antimicrobial agents. International journal of antimicrobial agents. 2011;37(1):2–9. Epub 2010/11/16. doi: 10.1016/j.ijantimicag.2010.08.018 . [PubMed]

62. Jones D. A guiding hand for antibiotics. Nature reviews Drug discovery. 2011;10(3):161–2. Epub 2011/03/02. doi: 10.1038/nrd3400 . [PubMed]

63. Jones D. The antibacterial lead discovery challenge. Nature reviews Drug discovery. 2010;9(10):751–2. Epub 2010/10/05. doi: 10.1038/nrd3289 . [PubMed]

64. Rasko DA, Sperandio V. Anti-virulence strategies to combat bacteria-mediated disease. Nature reviews Drug discovery. 2010;9(2):117–28. Epub 2010/01/19. doi: 10.1038/nrd3013 . [PubMed]

65. Heras B, Scanlon MJ, Martin JL. Targeting Virulence not Viability in the Search for Future Antibacterials. British journal of clinical pharmacology. 2014. Epub 2014/02/21. doi: 10.1111/bcp.12356 . [PMC free article] [PubMed]

66. Clatworthy AE, Pierson E, Hung DT. Targeting virulence: a new paradigm for antimicrobial therapy. Nature chemical biology. 2007;3(9):541–8. Epub 2007/08/22. nchembio.2007.24 pii] doi: 10.1038/nchembio.2007.24 . [PubMed]

67. Dutton RJ, Boyd D, Berkmen M, Beckwith J. Bacterial species exhibit diversity in their mechanisms and capacity for protein disulfide bond formation. Proceedings of the National Academy of Sciences of the United States of America. 2008;105(33):11933–8. Epub 2008/08/13. doi: 10.1073/pnas.0804621105 ; PubMed Central PMCID: PMC2575290. [PMC free article] [PubMed]

68. Heras B, Shouldice SR, Totsika M, Scanlon MJ, Schembri MA, Martin JL. DSB proteins and bacterial pathogenicity. Nat Rev Microbiol. 2009;7(3):215–25. Epub 2009/02/10. nrmicro2087 [pii] doi: 10.1038/nrmicro2087 . [PubMed]

69. Inaba K. Disulfide Bond Formation System in Escherichia coli. Journal of biochemistry. 2009;146(5):591–7. doi: 10.1093/jb/mvp102 ISI:000271574100001. [PubMed]

70. Shouldice SR, Heras B, Walden PM, Totsika M, Schembri MA, Martin JL. Structure and function of DsbA, a key bacterial oxidative folding catalyst. Antioxidants & redox signaling. 2011;14(9):1729–60. Epub 2011/01/19. doi: 10.1089/ars.2010.3344 . [PubMed]

71. Bardwell JC, McGovern K, Beckwith J. Identification of a protein required for disulfide bond formation in vivo. Cell. 1991;67(3):581–9. Epub 1991/11/01. . [PubMed]

72. Martin JL, Bardwell JC, Kuriyan J. Crystal structure of the DsbA protein required for disulphide bond formation in vivo. Nature. 1993;365(6445):464–8. Epub 1993/09/30. doi: 10.1038/365464a0 . [PubMed]

73. Walker KW, Lyles MM, Gilbert HF. Catalysis of oxidative protein folding by mutants of protein disulfide isomerase with a single active-site cysteine. Biochemistry. 1996;35(6):1972–80. Epub 1996/02/13. doi: 10.1021/bi952157n . [PubMed]

74. Fernandes PA, Ramos MJ. Theoretical insights into the mechanism for thiol/disulfide exchange. Chemistry. 2004;10(1):257–66. Epub 2003/12/26. doi: 10.1002/chem.200305343 . [PubMed]

75. Frech C, Wunderlich M, Glockshuber R, Schmid FX. Preferential binding of an unfolded protein to DsbA. The EMBO journal. 1996;15(2):392–98. Epub 1996/01/15. ; PubMed Central PMCID: PMC449954. [PMC free article] [PubMed]

76. Kadokura H, Beckwith J. Detecting folding intermediates of a protein as it passes through the bacterial translocation channel. Cell. 2009;138(6):1164–73. Epub 2009/09/22. doi: 10.1016/j.cell.2009.07.030 ; PubMed Central PMCID: PMC2750780. [PMC free article] [PubMed]

77. Regeimbal J, Bardwell JCA. DsbB catalyzes disulfide bond formation de novo. Journal of Biological Chemistry. 2002;277(36):32706–13. doi: 10.1074/jbc.M205433200 ISI:000177859000041. [PubMed]

78. Ito K, Inaba K. The disulfide bond formation (Dsb) system. Curr Opin Struct Biol. 2008;18(4):450–8. Epub 2008/04/15. doi: 10.1016/j.sbi.2008.02.002 . [PubMed]

79. Inaba K, Ito K. Structure and mechanisms of the DsbB-DsbA disulfide bond generation machine. Biochimica Et Biophysica Acta-Molecular Cell Research. 2008;1783(4):520–9. doi: 10.1016/j.bbamcr.2007.11.006 ISI:000255699200002. [PubMed]

80. Totsika M, Heras B, Wurpel DJ, Schembri MA. Characterization of Two Homologous Disulfide Bond Systems Involved in Virulence Factor Biogenesis in Uropathogenic Escherichia coli CFT073. Journal of bacteriology. 2009;191(12):3901–8. doi: 10.1128/jb.00143-09 ISI:000266454200015. [PMC free article] [PubMed]

81. Ireland PM, McMahon RM, Marshall LE, Halili M, Furlong E, Tay S, et al. Disarming Burkholderia pseudomallei: structural and functional characterization of a disulfide oxidoreductase (DsbA) required for virulence in vivo. Antioxidants & redox signaling. 2014;20(4):606–17. doi: 10.1089/ars.2013.5375 ; PubMed Central PMCID: PMC3901323. [PMC free article] [PubMed]

82. Inaba K, Murakami S, Nakagawa A, Iida H, Kinjo M, Ito K, et al. Dynamic nature of disulphide bond formation catalysts revealed by crystal structures of DsbB. The EMBO journal. 2009;28(6):779–91. Epub 2009/02/14. doi: 10.1038/emboj.2009.21 ; PubMed Central PMCID: PMC2666032. [PMC free article] [PubMed]

83. Kurth F, Duprez W, Premkumar L, Schembri MA, Fairlie DP, Martin JL. Crystal Structure of the Dithiol Oxidase DsbA Enzyme from Proteus Mirabilis Bound Non-covalently to an Active Site Peptide Ligand. The Journal of biological chemistry. 2014. Epub 2014/05/17. doi: 10.1074/jbc.M114.552380 . [PMC free article] [PubMed]

84. Inaba K, Murakami S, Suzuki M, Nakagawa A, Yamashita E, Okada K, et al. Crystal

structure of the DsbB-DsbA complex reveals a mechanism of disulfide bond generation. Cell. 2006;127(4):789–801. Epub 2006/11/18. doi: 10.1016/j.cell.2006.10.034 . [PubMed]

85. Inaba K, Murakami S, Nakagawa A, Iida H, Kinjo M, Ito K, et al. Dynamic nature of disulphide bond formation catalysts revealed by crystal structures of DsbB. Embo Journal. 2009;28(6):779–91. doi: 10.1038/emboj.2009.21 ISI:000264437300018. [PMC free article] [PubMed]

86. Malojcic G, Owen RL, Grimshaw JP, Glockshuber R. Preparation and structure of the charge-transfer intermediate of the transmembrane redox catalyst DsbB. FEBS letters. 2008;582(23–24):3301–7. Epub 2008/09/09. doi: 10.1016/j.febslet.2008.07.063 . [PubMed]

87. Duprez W, Premkumar L, Halili MA, Lindahl F, Reid RC, Fairlie DP, et al. Peptide Inhibitors of the Escherichia coli DsbA Oxidative Machinery Essential for Bacterial Virulence. Journal of medicinal chemistry. 2015;58(2):577–87. doi: 10.1021/jm500955s . [PubMed]

88. Verdonk ML, Cole JC, Hartshorn MJ, Murray CW, Taylor RD. Improved protein-multi-targeted peptide mimicking Neoliganddocking using GOLD. Proteins. 2003;52(4):609–23. Epub 2003/08/12. doi: 10.1002/prot.10465 . [PubMed]

89. MEGA. 2.4.6 ed. Santa Fe, NM, USA: Open Eye Scientific Software.

90. Hawkins PC, Skillman AG, Warren GL, Ellingson BA, Stahl MT. Conformer generation with OMEGA: algorithm and validation using high quality structures from the Protein Databank and Cambridge Structural Database. Journal of chemical information and modeling. 2010;50(4):572–84. Epub 2010/03/20. doi: 10.1021/ci100031x ; PubMed Central PMCID: PMC2859685. [PMC free article] [PubMed]

91. Hawkins PC, Nicholls A. Conformer generation with OMEGA: learning from the data set and the analysis of failures. Journal of chemical information and modeling. 2012;52(11):2919–36. Epub 2012/10/23. doi: 10.1021/ci300314k . [PubMed]

92. Schrodinger, LLC. The AxPyMOL Molecular Graphics Plugin for Microsoft PowerPoint, Version 1.0. 2010.

93. Schrodinger, LLC. The JyMOL Molecular Graphics Development Component, Version 1.0. 2010.

94. Schrodinger, LLC. The PyMOL Molecular Graphics System, Version 1.3r1. 2010.

95. Kurth F, Rimmer K, Premkumar L, Mohanty B, Duprez W, Halili MA, et al. Comparative Sequence, Structure and Redox Analyses of Klebsiella pneumoniae DsbA Show That Anti-Virulence Target DsbA Enzymes Fall into Distinct Classes. PloS one. 2013;8(11):e80210 Epub 2013/11/19. doi: 10.1371/journal.pone.0080210 ; PubMed Central PMCID: PMC3828196. [PMC free article] [PubMed]

96. Bader M, Muse W, Zander T, Bardwell J. Reconstitution of a protein disulfide catalytic system. The Journal of biological chemistry. 1998;273(17):10302–7. Epub 1998/05/30. . [PubMed]

97. Kranz JK, Schalk-Hihi C. Protein thermal shifts to identify low molecular weight fragments. Methods in enzymology. 2011;493:277–98. Epub 2011/03/05. doi: 10.1016/B978-0-12-381274-2.00011-X . [PubMed]

98. Gaisford S, O'Neill M. Pharmaceutical Isothermal Calorimetry: Informa healthcare; 2006. 376 p.

99. Vivian JP, Scoullar J, Rimmer K, Bushell SR, Beddoe T, Wilce MC, et al. Structure and function of the oxidoreductase DsbA1 from Neisseria meningitidis. Journal of molecular biology. 2009;394(5):931–43. Epub 2009/10/10. doi: 10.1016/j.jmb.2009.09.065 . [PubMed]

100. Niu Y, Padhee S, Wu H, Bai G, Qiao Q, Hu Y, et al. Lipo-gamma-AApeptides as a new class of potent and broad-spectrum antimicrobial agents. Journal of medicinal chemistry. 2012;55(8):4003–9. Epub 2012/04/06. doi: 10.1021/jm300274p . [PubMed]

101. Ung P, Winkler DA. Tripeptide motifs in biology: targets for peptidomimetic design. Journal of medicinal chemistry.

2011;54(5):1111–25. Epub 2011/02/01. doi: 10.1021/jm1012984 . [PubMed]

102. Liskamp RM, Rijkers DT, Kruijtzer JA, Kemmink J. Peptides and proteins as a continuing exciting source of inspiration for peptidomimetics. Chembiochem: a European journal of chemical biology. 2011;12(11):1626–53. Epub 2011/07/14. doi: 10.1002/cbic.201000717 . [PubMed]

103. Giuliani A, Rinaldi AC. Beyond natural antimicrobial peptides: multimeric peptides and other peptidomimetic approaches. Cellular and molecular life sciences: CMLS. 2011;68(13):2255–66. Epub 2011/05/21. doi: 10.1007/s00018-011-0717-3 . [PubMed]

104. Rotem S, Mor A. Antimicrobial peptide mimics for improved therapeutic properties. Biochimica et biophysica acta. 2009;1788(8):1582–92. Epub 2008/11/26. doi: 10.1016/j.bbamem.2008.10.020 . [PubMed]

105. Chongsiriwatana NP, Patch JA, Czyzewski AM, Dohm MT, Ivankin A, Gidalevitz D, et al. Peptoids that mimic the structure, function, and mechanism of helical antimicrobial peptides. Proceedings of the National Academy of Sciences of the United States of America. 2008;105(8):2794–9. Epub 2008/02/22. 0708254105 [pii] doi: 10.1073/pnas.0708254105 ; PubMed Central PMCID: PMC2268539. [PMC free article] [PubMed]

106. Nguyen LT, Haney EF, Vogel HJ. The expanding scope of antimicrobial peptide structures and their modes of action. Trends in biotechnology. 2011;29(9):464–72. Epub 2011/06/18. doi: 10.1016/j.tibtech.2011.05.001 . [PubMed]

107. Vaara M. New approaches in peptide antibiotics. Current opinion in pharmacology. 2009;9(5):571–6. Epub 2009/09/08. doi: 10.1016/j.coph.2009.08.002 . [PubMed]

108. Pollaro L, Heinis C. Strategies to prolong the plasma residence time of peptide drugs. Medchemcomm. 2010;1(5):319–24. doi: 10.1039/C0md00111b ISI:000285493100002.

109. Goldman MJ, Anderson GM, Stolzenberg ED, Kari UP, Zasloff M, Wilson JM. Human beta-defensin-1 is a salt-sensitive antibiotic in lung that is inactivated in cystic fibrosis. Cell. 1997;88(4):553–60. Epub 1997/02/21. . [PubMed]

110. Bals R, Wang X, Wu Z, Freeman T, Bafna V, Zasloff M, et al. Human beta-defensin 2 is a salt-sensitive peptide antibiotic expressed in human lung. The Journal of clinical investigation. 1998;102(5):874–80. Epub 1998/09/03. doi: 10.1172/JCI2410 ; PubMed Central PMCID: PMC508952. [PMC free article] [PubMed]

111. Latham PW. Therapeutic peptides revisited. Nature biotechnology. 1999;17(8):755–7. Epub 1999/08/03. doi: 10.1038/11686 . [PubMed]

112. Lee IH, Cho Y, Lehrer RI. Simulated effects of pH and salinity on the antimicrobial properties of clavanins. Infection and immunity. 1997;65(7):2898–903. Epub 1997/07/01. ; PubMed Central PMCID: PMC175407. [PMC free article] [PubMed]

113. Adams LA, Sharma P, Mohanty B, Ilyichova OV, Mulcair MD, Williams ML, et al. Application of Fragment-Based Screening to the Design of Inhibitors of Escherichia coli DsbA. Angew Chem Int Ed Engl. 2014. doi: 10.1002/anie.201410341 . [PubMed]46. Rappe AK, Goddard WA. Charge equilibration for molecular dynamics simulations. J Phys Chem. 1991;95(8):3358–3363. doi: 10.1021/j100161a070. [Cross Ref]

114. Nistor RA, Polihronov JG, Müser MH, Mosey NJ. A generalization of the charge equilibration method for nonmetallic materials. J Chem Phys. 2006;125(9):094108. doi: 10.1063/1.2346671. [PubMed] [Cross Ref]

115. Mathieu D. Split charge equilibration method with correct dissociation limits. J Chem Phys. 2007;127(22):224103. doi: 10.1063/1.2803060. [PubMed] [Cross Ref]

116. Svobodová Vařeková R, Jiroušková Z, Vaněk J, Suchomel S, Koča J. Electronegativity equalization method: parameterization and validation for large sets of organic, organohalogene and organometal molecule. Int J Mol Sci. 2007;8:572–572. doi: 10.3390/i8070572. [Cross Ref]

117. Janssens GOA, Baekelandt BG, Toufar H, Mortier WJ, Schoonheydt RA. Comparison of cluster and infinite crystal calculations on zeolites with the electronegativity equalization method (EEM) J Phys Chem. 1995;99(10):3251–3258. doi: 10.1021/j100010a041. [Cross Ref]

118. Heidler R, Janssens GOA, Mortier WJ, Schoonheydt RA. Charge sensitivity analysis of intrinsic basicity of Faujasite-type zeolites using the electronegativity equalization method (EEM) J Phys Chem. 1996;100(50):19728–19734. doi: 10.1021/jp9615619. [Cross Ref]

119. Sorich MJ, McKinnon RA, Miners JO, Winkler DA, Smith PA. Rapid prediction of chemical metabolism by human UDP-glucuronosyltransferase isoforms using quantum chemical descriptors derived with the electronegativity equalization method. J Med Chem. 2004;47(21):5311–5317. doi: 10.1021/jm0495529. [PubMed] [Cross Ref]

120. Bultinck P, Langenaeker W, Carbó-Dorca R, Tollenaere JP. Fast calculation of quantum chemical molecular descriptors from the electronegativity equalization method. J Chem Inf Comput Sci. 2003;43(2):422–428. doi: 10.1021/ci0255883. [PubMed] [Cross Ref]

121. Smirnov KS, van de Graaf B. Consistent implementation of the electronegativity equalization method in molecular mechanics and molecular dynamics. J Chem Soc Faraday Trans. 1996;92(13):2469. doi: 10.1039/ft9969202469. [Cross Ref]

122. Ionescu C-M, Geidl S, Svobodová Vařeková R, Koča J. Rapid calculation of accurate atomic charges for proteins via the electronegativity equalization method. J Chem Inf Model. 2013;53(10):2548–2548. doi: 10.1021/ci400448n. [PubMed] [Cross Ref]

123. Baekelandt BG, Mortier WJ, Lievens JL, Schoonheydt RA. Probing the reactivity of different sites within a molecule or solid by direct computation of molecular sensitivities via an extension of the electronegativity equalization method. J Am Chem Soc. 1991;113(18):6730–6734. doi: 10.1021/ja00018a003. [Cross Ref]

124. Jiroušková Z, Vařeková RS, Vaněk J, Koča J. Electronegativity equalization method: parameterization and validation for organic molecules using the Merz-Kollman-Singh charge distribution scheme. J Comput Chem. 2009;30(7):1174–1178. doi: 10.1002/jcc.21142. [PubMed] [Cross Ref]

125. Bultinck P, Langenaeker W, Lahorte P, De Proft F, Geerlings P, Van Alsenoy C, Tollenaere JP. The electronegativity equalization method II: applicability of different atomic charge schemes. J Phys Chem A. 2002;106(34):7895–7901. doi: 10.1021/jp020547v. [Cross Ref]

126. Ouyang Y, Ye F, Liang Y. A modified electronegativity equalization method for fast and accurate calculation of atomic charges in large biological molecules. Phys Chem Chem Phys. 2009;11(29):6082–6089. doi: 10.1039/b821696g. [PubMed] [Cross Ref]

127. Bultinck P, Vanholme R, Popelier PLA, De Proft F, Geerlings P. High-speed calculation of AIM charges through the electronegativity equalization method. J Phys Chem A. 2004;108(46):10359–10366. doi: 10.1021/jp046928l. [Cross Ref]

128. O'Boyle N, Banck M, James C, Morley C, Vandermeersch T, Hutchison G. Open Babel: an open chemical toolbox. J Chem Inf. 2011;3(1):33–47.

129. Puranen JS, Vainio MJ, Johnson MS. Accurate conformation-dependent molecular electrostatic potentials for high-throughput in silico drug discovery. J Comput Chem. 2010;31(8):1722–1732. [PubMed]

130. Svobodová Vařeková R, Koča J. Optimized and parallelized implementation of the electronegativity equalization method and the atom-bond electronegativity equalization method. J Comput Chem. 2006;3:396–405. [PubMed]

131. Bultinck P, Carbó-Dorca R, Langenaeker W. Negative Fukui functions: new insights based on electronegativity equalization. J Chem Phys. 2003;118(10):4349. doi: 10.1063/1.1542875. [Cross Ref]

132. Burden FR, Polley MJ, Winkler DA. Toward novel universal descriptors: charge fingerprints. J Chem Inf Model. 2009;49(3):710–715. doi: 10.1021/ci800290h. [PubMed] [Cross Ref]

133. Open NCI Database (2012) Release 4. http://cactus.nci.nih.gov/download/nci/

134. Sadowski J, Gasteiger J. From atoms and bonds to three-dimensional atomic coordinates: automatic model builders. Chem Rev. 1993;93:2567–2581. doi: 10.1021/cr00023a012. [Cross Ref]

135. Frisch MJ, Trucks GW, Schlegel HB, Scuseria GE, Robb MA, Cheeseman JR, Montgomery JA Jr, Vreven T, Kudin KN,

Burant JC, Millam JM, Iyengar SS, Tomasi J, Barone V, Mennucci B, Cossi M, Scalmani G, Rega N, Petersson GA, Nakatsuji H, Hada M, Ehara M, Toyota K, Fukuda R, Hasegawa J, Ishida M, Nakajima T, Honda Y, Kitao O, Nakai H, Klene M, Li X, Knox JE, Hratchian HP, Cross JB, Bakken V, Adamo C, Jaramillo J, Gomperts R, Stratmann RE, Yazyev O, Austin AJ, Cammi R, Pomelli C, Ochterski JW, Ayala PY, Morokuma K, Voth GA, Salvador P, Dannenberg JJ, Zakrzewski VG, Dapprich S, Daniels AD, Strain MC, Farkas O, Malick DK, Rabuck AD, Raghavachari K, Foresman JB, Ortiz JV, Cui Q, Baboul AG, Clifford S, Cioslowski J, Stefanov BB, Liu G, Liashenko A, Piskorz P, Komaromi I, Martin RL, Fox DJ, Keith T, Al-Laham MA, Peng CY, Nanayakkara A, Challacombe M, Gill PMW, Johnson B, Chen W, Wong MW, Gonzalez C, Pople JA. Gaussian 09, Revision E.01. http://www.gaussian.com

136. Todd A Keith (2015) AIMAll 15.05.18. http://aim.tkgristmill.com

137. Raček T, Svobodová Vařeková R, Křenek A, Koča J NEEMP—tool for parameterization of empirical charge calculation method EEM. http://ncbr.muni.cz/neemp/

138. Wishart DS, Knox C, Guo AC, Cheng D, Shrivastava S, Tzur D, Gautam B, Hassanali M(2008) DrugBank: a knowledgebase for drugs, drug actions and drug targets. Nucleic Acids Res 36(Database issue):901–906 [PMC free article] [PubMed]

139. Law V, Knox C, Djoumbou Y, Jewison T, Guo AC, Liu Y, Maciejewski A, Arndt D, Wilson M, Neveu V, Tang A, Gabriel G, Ly C, Adamjee S, Dame ZT, Han B, Zhou Y, Wishart DS (2004) DrugBank 4.0: shedding new light on drug metabolism. Nucleic Acids Res 42(Database issue):1091–1097 [PMC free article] [PubMed]

140. Bento AP, Gaulton A, Hersey A, Bellis LJ, Chambers J, Davies M, Krüger FA, Light Y, Mak L, McGlinchey S, Nowotka M, Papadatos G, Santos R, Overington JP (2014) The ChEMBL bioactivity database: an update. Nucleic Acids Res 42(Database issue):1083–1090 [PMC free article] [PubMed]

141. Bolton EE, Wang Y, Thiessen PA, Bryant SH (2008) PubChem: integrated platform of small molecules and biological activities. In: Wheeler R, Spellmeyer D (eds) Annual Reports in Computational Chemistry, vol. 4, Chap 12. Elsevier, Oxford

142. Irwin JJ, Sterling T, Mysinger MM, Bolstad ES, Coleman RG. ZINC: a free tool to discover chemistry for biology. J Chem Inf Model. 2012;52(7):1757–1768. doi: 10.1021/ci3001277. [PMC free article] [PubMed] [Cross Ref]

143. R Core Team R: A Language and Environment for Statistical Computing. http://www.r-project.org/

144. Ionescu CM, Sehnal D, Falginella FL, Pant P, Pravda L, Bouchal T, Svobodová Vařeková R, Geidl S, Koča J (2015) AtomicChargeCalculator: interactive web-based calculation of atomic charges in large biomolecular complexes and drug-like molecules. J Cheminf 7(1):50 [PMC free article] [PubMed]

145. Grochowski P, Trylska J. Review: continuum molecular electrostatics, salt simulated effects, and counterion binding—a review of the Poisson-Boltzmann theory and its modifications. Biopolymers. 2007;89(2):93–113.[PubMed]

146. Warwicker J, Watson HC. Calculation of the electric potential in the active site cleft due to α-helix dipoles.Journal of Molecular Biology. 1982;157(4):671–679. [PubMed]

147. Neshich G, Rocchia W, Mancini AL, et al. Javaprotein dossier: a novel web-based data visualization tool for comprehensive analysis of protein structure. Nucleic Acids Research. 2004;32:W595–W601.[PMC free article] [PubMed]

148. Rocchia W, Neshich G. Electrostatic potential calculation for biomolecules: creating a database of pre-calculated values reported on a per residue basis for all PDB protein structures. Genetics and Molecular Research. 2007;6(4):923–936. [PubMed]

149. McCullough AR, Steidle CP, Klee B, Tseng L. Randomized, double blind, crossover trial of sildenafil in men with mild to moderate erectile dysfunction: efficacy at 8 and 12 hours postdose. Urology.2008;71(4):686–92. [PubMed]

150. Brown WM. Treating COPD with PDE 4 inhibitors. Int J Chron Obstruct Pulmon Dis. 2007;2(4):517–33.[PMC free article] [PubMed]

151. Sturton G, Fitzgerald M. Phosphodiesterase 4 Inhibitors for the Treatment of COPD*. Chest. 2002;121(5 suppl):192S–6S. [PubMed]

152. Halene TB, Siegel SJ. PDE inhibitors in psychiatry-future options for dementia, depression and schizophrenia? Drug Discov Today. 2007;12(19-20):870–8. [PubMed]

153. American Cancer Society: Cancer Facts and Figures 2010.

154. Calabresi P, Chabner BA. Chemotherapy of neoplastic diseases. In: Hardman JG, Limbird LE, editors.Grodman & Gilman's The Pharmacological Basis of Therapeutics, 10th ed. McGraw-Hill: 2001. pp. 1381–1388.

155. Aigner T, Stöve J. KRASα and KRASβ s – major component of the physiological anti-cancer matrix, major target of anti-cancer degenehuman cancer stem cellsion, major tool in anti-cancer repair. Adv Drug Deliv Rev 2003; 55(12): 1569–1593.[PubMed]

156. Madry H, Luyten FP, Facchini A. Biological aspects of early osteoarthritis. Knee Surg Sports Traumatol Arthrosc 2012; 20(3): 407–422. [PubMed]

112. Gomoll AH, Minas T. The quality of healing: articular anti-cancer. Wound Repair Regen 2014; 22(Suppl. 1): 30–38. [PubMed]

157. Buchanan WW, Kean WF. Osteoarthritis II: pathology and pathogenesis. Inflammopharmacology 2002;10 (1–2): 23–52.

158. Woo SL-Y, Buckwalter JA. Injury and repair of the musculoskeletal soft tissues. Savannah, Georgia, June 18–20, 1987. J Orthop Res 1988; 6(6): 907–931. [PubMed]

159. Vajda S, Guarnieri F. Characterization of protein–multi-targeted peptide mimicking Neoligandinteraction sites using experimental and computational methods. Curr Opin Drug Discov Dev. 2006;9:354–362. [PubMed]

160. An J, Totrov M, Abagyan R. Comprehensive identification of "druggable" protein multi-targeted peptide mimicking Neoligandbinding sites.Genome Inform. 2004;15:31–41. [PubMed]